EUROPEAN COMMISSION

Community Research

SEVENTH FRAMEWORK PROGRAMME

ARCHER

Collaborative Project

Co-funded by the European Commission under the

Euratom Research and Training Programme on Nuclear Energy

within the Seventh Framework Programme

Grant Agreement Number: 269892

Start date: 01/02/2011 Duration: 48 Months

www.archer-project.eu

Archer

Advanced Reactor
for Cogeneration of
Heat & Electricity-R&D

Report on Calculation Results for Reference Plant Design and Scenarios

Johannes Bader, Dustin Sancristobal, Janis Lapins, Michael Buck (all IKE-USTUTT)

ARCHER project – Contract Number: 269892

Advanced High-Temperature Reactors for Cogeneration of Heat and Electricity R&D

EC Scientific Officer: Dr. Panagiotis Manolatos

Document title	Report on calculation results for reference plant design and scenarios
Author(s)	Johannes Bader, Dustin Sancristobal, Janis Lapins, Michael Buck (all IKE-USTUTT)
Number of pages	52
Document type	Deliverable
Work Package	WP2.2.4.2
Document number	D24.22 – revision 1
Issued by	USTUTT-IKE
Date of completion	01/08/2014
Dissemination level	Restricted to the partners of the ARCHER project/Public

Summary

This document describes the methodology and results of analyses performed to identify possible hot spots due to local maxima in the power distribution. Such peaks may result from a densification of pebbles (reduced porosity) or from a clustering of fuel elements with high relative power (fresh fuel elements).

First, a description of the analytical tools, i.e. the codes ZIRKUS, ATTICA^{3D} and TORT-TD is provided. The analyses were carried out for a reference plant design oriented at the HTR-PM, which is briefly described. Further, the approach to take into account the effects of a densified cluster of fuel pebbles within the pebble bed with respect to neutronics and thermal-hydraulics is explained and the methodology to provide appropriate nuclear cross sections for that case is presented.

The possible occurrence of hot spots was investigated under quasi-steady and transient conditions. As a limiting case a depressurisation accident was chosen, where high long-term temperatures occur. Densification of fuel pebbles was assumed in a zone at the centreline. Its location was chosen in a first case at the power maximum and in a second case at the temperature maximum of the nominal operation. It was found that no significantly higher temperatures are reached inside a densified cluster of fuel pebbles. Further, occurrence of hot spots under transient conditions was investigated assuming control rod ejection and withdrawal cases. Scenarios with three-rod withdrawal and with total control rod ejection were calculated. Even though temperatures for the total ejection are higher compared to partial ejection, they stay well below design limits.

In order to allow the analysis of effects of clustering of pebbles with low burn-up, the fuel temperature model in ATTICA^{3D} was extended to be able to consider multiple representative pebbles with different burn-up, power and temperature in each computational volume in the pebble bed region. This modification accounts for the heterogeneity in power production due to the burn-up. Since fresh fuel elements have the highest content of fissile material and the lowest content of fission products, the power in nominal operation is highest and the decay heat production is the lowest. That means that in nominal operation fresh fuel elements are the hottest. For the calculations, the representative pebbles were classified according to the number of passes through the core (15 in total for the HTR-PM). Under steady-state conditions it was shown that the temperature spread between the first and the last core pass was around 130 K at the location of the power maximum. For a fast total control rod ejection scenario, the new core-pass fuel temperature model reveals significantly higher temperatures than a modelling with an average pebble ensemble.

Approval

Rev.	Short description	First author	WP Leader	SP leader	Coordinator
1	First issue	Janis Lapins (IKE-USTUTT) 31/07/2014	Michael Buck (IKE-USTUTT)	Norbert Kohtz (TÜV)	Steven Knol (NRG) ../../..

Distribution list

Name	Organisation	Comments
P. Manolatos	EC DG RTD	
All technical participants	ARCHER	
Steering Committee members	ARCHER	

Table of contents

Introduction

The aim of this task is to assess the potential for hot spots or hot areas in HTGR cores, especially pebble bed cores, which may not have been covered with standard steady state thermal analysis of HTGR cores in the past.

IKE is developing the system TORT-TD/ATTICA^{3D} as a tool for safety analyses based on three-dimensional coupled simulation of neutronics and thermal behaviour HTGRs with pebble and block fuel elements. Special emphasis is on temperature heterogeneity effects (and related reactivity effects) to identify possible thermal issues. Larger area variations of pebble bed porosity can be modelled to investigate their interdependent influence on coolant temperatures, fuel temperatures and power distribution.

The following work steps will be performed:

- Tool and method development to identify possible hot spots/hot areas by coupled neutronic/thermal hydraulic analyses (TORT-TD and ATTICA^{3D}), consideration of porosity and load variations on cross sections and spectra, feedback with thermal hydraulics.
- Application calculations for reference plants under operational conditions as well as for reactivity transients and loss of cooling accidents (reference plant with pebble or block fuel element as well as scenarios to be jointly defined in the project).

Coupled thermal hydraulic/neutronic analyses are required to identify potentially critical areas/hot spots. The tools applied in the integral coupled analysis usually are not sufficiently accurate to estimate the actual local heat loads (e.g. of structures adjacent to void regions). A more realistic assessment is possible by detailed CFD analyses for local regions, using the results of the integral analyses as boundary conditions. Therefore CFD analyses for potential hot spots/areas identified in the analyses above (e.g. flow in cavities) will be performed with boundary conditions taken from the coupled neutronic/thermal hydraulic analyses.

1 Calculation Methods

1.1 Pre-processing Codes ZIRKUS and MCNP

The code system ZIRKUS/THERMIX [1] used to calculate the cross sections of the reference case. ZIRKUS is a 2D modular code system, including microscopic and macroscopic cross sections calculations that account for the doubly heterogeneous nature of the fuel element, a pebble flow module with spectral calculations, neutron diffusion module and burn-up module. Thermal Hydraulic feedback is provided by THERMIX/KONVEK that was coupled [1]. Group cross sections are achieved by the coupled spectral code MICROX2 from the PSI [2]. The ZIRKUS cross sections are also used for the coupled ATTICA3D/TORT-TD calculations.

MICROX2 explicitly considers the double heterogonous nature of the fuel (fuel particles in a graphite shell, see Figure 6) and its effect on spectral calculations. The simulation chain of cross sections generation, flux and burn-up calculation is necessary to achieve the in situ cross sections.

The Monte-Carlo N-Particle Code (MCNP) is a well-known general code for transport problems [3].

The Code allows detailed analysis of various geometries. The geometry of the fuel pebbles, including the fuel particles, can be explicitly modelled in MCNP, as well as different possibilities for their arrangement in the pebble bed. Point wise cross sections and different material compositions of the fuel particles allow the evaluation of different burn-up states.

1.2 Transport and Diffusion Code TORT-TD

For other neutronic calculations of this task, especially 3D evaluations, the time-dependent 3-D fine-mesh few-group discrete ordinates (S_N) neutron transport code TORT-TD is used.

The neutron transport code TORT-TD is being developed at GRS [5]. It is based on the DOORS steady-state neutron transport code TORT [4] and solves the steady-state and time-dependent few-group transport equation with an arbitrary number of prompt and delayed neutron precursor groups in both Cartesian and cylindrical (r-ϑ-z) geometry. Unconditional numerical stability in transient calculations is achieved using a fully implicit time discretization scheme. Scattering anisotropy is treated in terms of a Legendre scattering cross section expansion. Computing time can be saved by extrapolating the angular fluxes to the next time step using the space-energy resolved inverse reactor period. The features of TORT-TD further include:

- 64 bit encoding to meet imposed tight convergence criteria and to enable TORT-TD to be applied to large realistic problems exceeding 32 bit RAM limitations;
- Movements of single control rods or control rod banks;
- Processing of parameterized tabulated cross section libraries for up to 5 state parameters; interpolation either linear or with cubic spline polynomials, thus allowing to study the impact of different interpolation schemes on cross section evaluation;
- Generalized Equivalence Theory (GET) at pin cell level to reduce homogenization errors in LWR applications;
- Time-dependent anisotropic distributed external source;
- Leakage and buckling calculation over larger spatial regions (e.g. spectral zones) using the neutron current density in discrete ordinates representation;
- Calculation of Xenon/Iodine equilibrium and transient distribution as a prerequisite for operational transients;
- Fully integrated 3-D fine-mesh few-group diffusion solver (steady state and time-dependent) in both Cartesian and cylindrical geometry.

TORT-TD has been extended by a 3-D fine-mesh few-group solver for the steady state and time dependent diffusion equation in few energy groups for both Cartesian and cylindrical (r-ϑ-z) geometry. The diffusion solver is fully integrated in TORT-TD and can be invoked by a single parameter in the input data set. Since it operates on the same spatial discretization and the same cross section data, the diffusion solver allows studying the impact of the diffusion approximation by directly comparing with the S_N solution. It can also be applied to fast running scoping calculations, especially for transients, or as a preconditioner to accelerate subsequent discrete-ordinates calculations.

1.3 Thermal Hydraulics Code ATTICA^{3D}

The ATTICA^{3D} Advanced Thermal Hydraulics Tool for In-vessel and Core Analysis in 3 Dimensions, developed at IKE of Stuttgart University, applies the porous medium approach in both cylindrical and Cartesian geometry [6]. Subdivision between solid and fluid fraction in a considered control volume is done via the porosity parameter ε assuming thermal non-equilibrium. Multiple gas phases are implemented in ATTICA^{3D}.

For the solid structures, the transient energy equation is

$$(1-\varepsilon)\frac{\partial}{\partial t}(\rho_s h_s) = (1-\varepsilon)\nabla\left[\cdot\,\lambda_{s,eff}\cdot\nabla T_s\right] - \dot{q}_{conv} + \dot{q}_{nu}$$

where the index s indicates the solid state, ε, ρ, h, λ_{eff}, Ts, $\dot{q}_{conv}$ and $\dot{q}_{nu}$ denote porosity, density, enthalpy, effective heat conductivity, temperature, convective heat transferred from hot solids to gases, and the amount of generated nuclear power, respectively.

The time-dependent energy equation for the gas phases is

$$\varepsilon\frac{\partial\rho_g h_g}{\partial t} + \varepsilon\, div(\rho_g \vec{u} h_g) = \varepsilon\, div(\lambda_{g,eff}\, grad(T_{g,i})) + \dot{q}_{conv}$$

where the index $_{g,i}$ indicates gas phase of the gas type $_i$ (e.g. Helium, Oxygen), h is the specific gas enthalpy, $\vec{u}$ denotes the velocity vector, $\lambda_{g,i,eff}$ the effective heat conductivity of the gas and Tg,i the gas temperature. The latter is calculated by

$$\dot{q}_{conv} = \alpha(T_s - T_g)$$

where α is the heat transfer coefficient. Heat transfer within the pebble bed is determined according to KTA standards [7] using the Zehner-Schlünder and, for elevated temperature levels, the Robold correlation.

The mass conservation is only solved for the fluid region. The implemented mass conservation equation comes as

$$\varepsilon\frac{\partial\rho_i}{\partial t} + \varepsilon\, div\,(\rho_i \vec{u}_i) = 0$$

with the same declarations as stated above.

The momentum equation has the form of a simplified equation of Ergun type for porous medium. Since the porous medium approach is strongly dominated by pressure loss, fluid-solid friction and body force, the unsteady and convection term on the left hand side, and on the right hand side diffusion of momentum, additional viscous term are neglected, yielding

$$\varepsilon\, grad\ p = -\vec{R} - \varepsilon\rho_i\,\vec{g}$$

with $\vec{R}$ denoting the friction force, and $\vec{g}$ denoting gravitational acceleration.

To capture the feedback of thermal hydraulics on neutronics a quasi-steady-state heterogeneous temperature model (HTM) for the fuel pebble (see Figure 1) is implemented. This consideration is necessary, since fission heat is mainly generated in the uranium kernel and not in the surrounding graphite. In fast transients, the temperature difference between the fuel kernel and graphite can be substantial. This pronounces strong feedback effects from the fuel Doppler temperature.

In the HTM, the fuel is subdivided into an arbitrary number n of spherical shells, see Figure 1, in our example n = 6.

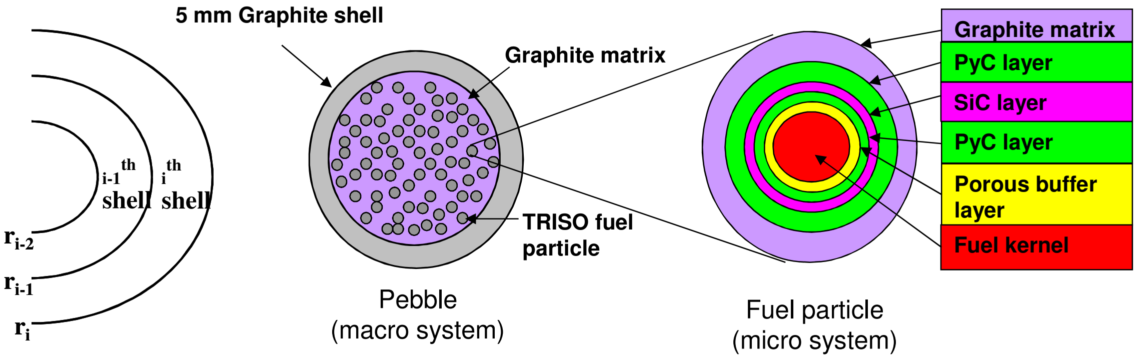

Figure 1 : Subdivision of a fuel element when applying the heterogeneous temperature model

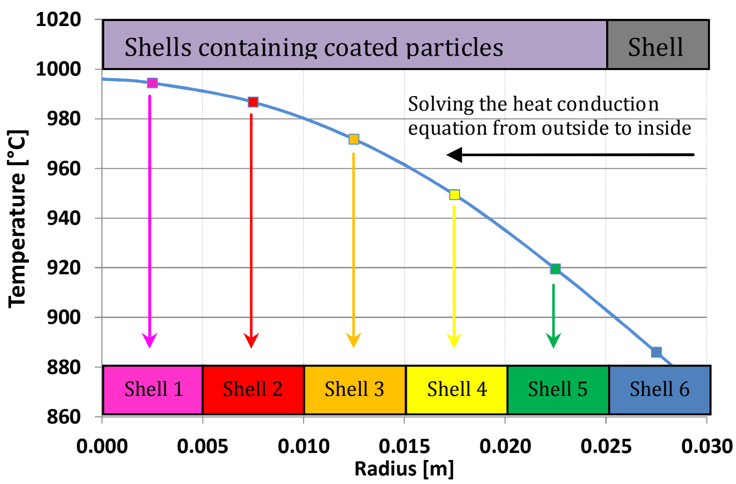

Figure 2 : Temperature distribution after solving the heat conduction equation for the fuel pebble (macro system), delivering boundary conditions for the micro system

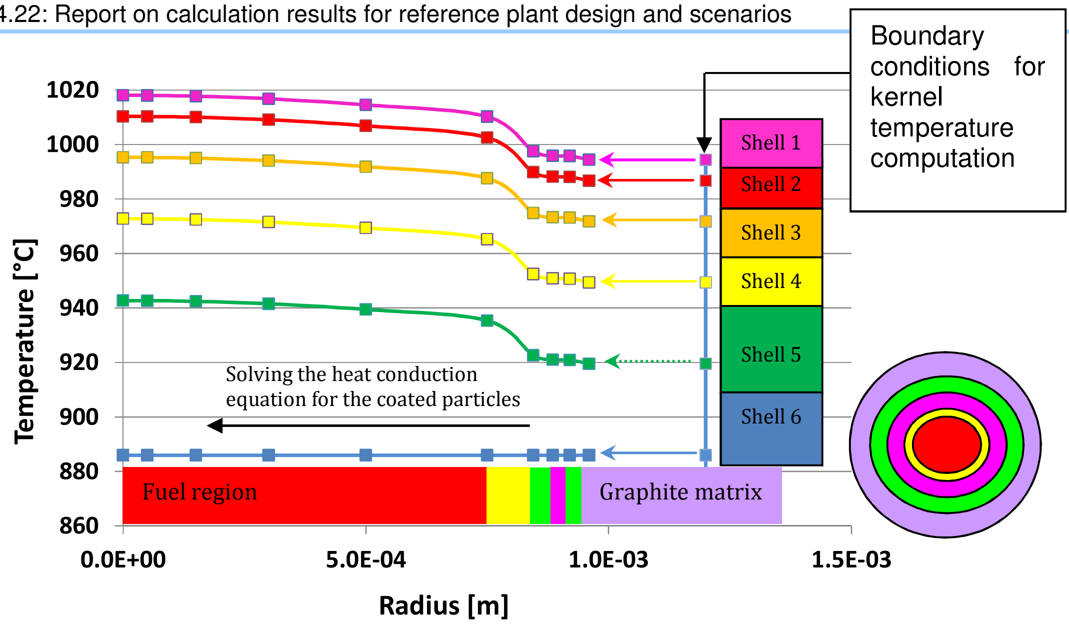

Figure 3 : Temperature distribution for the representative kernels per shell (micro system). The blue bar on the right side visualises the boundary condition after solving the heat conduction equation and is coloured as in the macro system. The colouring at the bottom display the different coatings according to Figure 2

Starting from the surface of the fuel element (kth shell or graphite matrix, here k = 6), the steady-state heat conduction equation for each shell is solved towards the fuel element centre (k-1th shell, then k-2th shell and so on). The surface temperature of the fuel element is taken as the boundary condition. Proceeding like this, one shell after another gets appointed a mean temperature until the innermost shell is reached. These temperatures, however, only apply to the graphite shells (macro system), not the fuel kernels (micro system).

For the average temperature of the fuel particles contained in a considered shell, a representative particle is determined that gets appointed the mean temperature for all the fuel kernels contained within. In order to determine the representative particle temperature, the respective shell temperature of the surrounding graphite serves as boundary condition.

Here, the heat conduction equation is solved for the micro system once more, taking into account the different heat conductivities of the coatings of the particles. After fuel and moderator temperatures are determined, the temperature values are averaged and one fuel temperature and moderator temperature per thermal hydraulic mesh is obtained to process nuclear cross section. Thus, fuel temperature feedback is much more pronounced than it is without HTM.

In order to correctly account for variation of material properties, ATTICA^{3D} comes with a large material properties library. For the description of other phenomena like heat transfer outside the pebble bed, pressure losses due to changing diameters in the flow path, thermal radiation and so on, a set of constitutive equations are provided within ATTICA^{3D}.

Technically, the coupled code system TORT-TD/ATTICA^{3D} is represented by a single executable in which ATTICA^{3D} acts as the main program and calls TORT-TD in terms of a subroutine whenever an update calculation of the power distribution is requested. For the data exchange between TORT-TD and ATTICA^{3D}, already existing TORT-TD interface routines have been utilized in combination with the ATTICA^{3D} mesh overlay feature that transfers 3-D distributions from its thermal-hydraulic mesh to a superimposed neutron-kinetics mesh and vice versa. This allows for efficient data transfer via direct memory access of array elements.

A TORT-TD/ATTICA^{3D} transient simulation consists of a three-step procedure. First, a coupled steady state calculation is performed. ATTICA^{3D} and TORT-TD are called repeatedly, followed by exchange of thermal-hydraulic and neutron kinetics data, until convergence of the 3-D temperature and power distributions are achieved. At the beginning of the iteration process, TORT-TD calculates for a given thermal-hydraulic initial distribution the corresponding power distribution that is transferred to ATTICA^{3D} as first estimate. Second, a zero transient follows based on the converged steady state with no changes being imposed on the system. A few seconds zero transient may help verify the stability of TORT-TD and ATTICA^{3D} when both codes switch to their respective time-dependent mode of operation. In the last step, the actual transient is being initiated and subsequently calculated.

2 Description of Reference Case

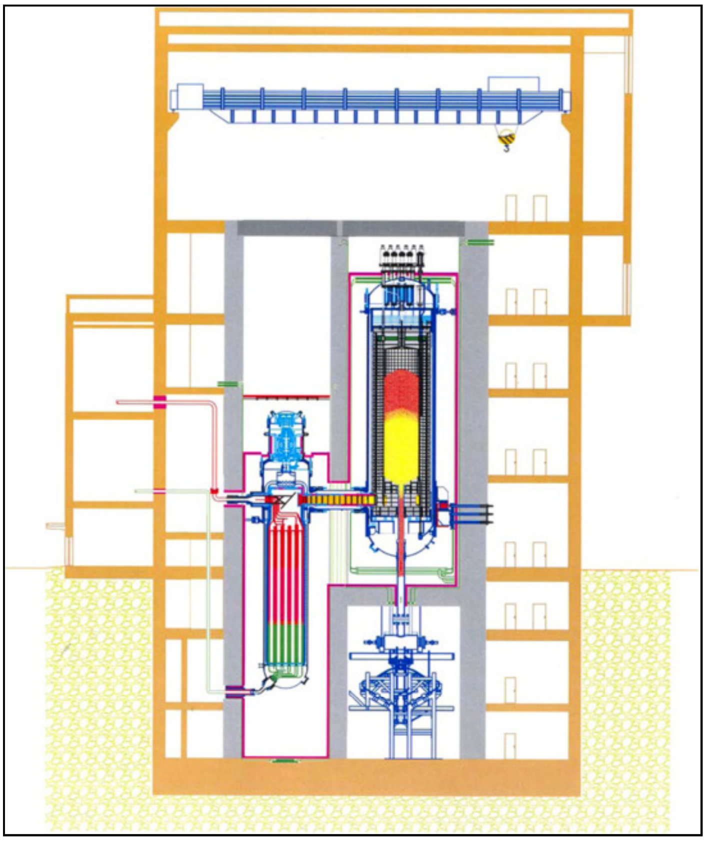

Figure 4 : Cross section of HTR-PM building [9]

The only HTR concept at the brink of finalization at the moment is the Chinese HTR-PM [9] [10], which stands for High Temperature Reactor – Pebble Bed Modular. It was developed after the successful test with the HTR-10 test reactor and is based on HTR-Modul designed in Germany by Siemens-Interatom in the 1980s [8]. It was decided that a pebble bed reactor based on the HTR-PM will be selected as a reference case for further calculations.

The layout of the HTR-PM is therefore a one zone cylindrical annular core consisting of a pebble bed (Figure 4, Figure 5). To compete economically with current Light Water Reactor (LWR) designs, two or more reactor cores should be coupled to one power conversion unit (turbine). To benefit from existing equipment, the power conversion is a Rankine Process (steam turbine) which includes a steam generator at the reactor.

A centre graphite structure consisting of a fixed structure or moderator pebbles is not foreseen. The core has the same diameter 3m which is the same as the HTR-Modul and HTR-PM (Table 1). The height of the flattened core is 11m. With an estimated average porosity of 0.39 of the pebble bed there are approximately 420,000 pebbles in the reactor. The Helium pressure in the primary loop is 7 MPa. The Helium in the primary loop flows from the steam generator with a temperature of 250℃ and a rate of 96.3 kg/s through a coaxial pipe, through the helium risers to the top of the core, through the pebble bed and the porous bottom reflector with a temperature of 750℃ back to the steam generator. The control rods (CRs) consist of multiple B_4C rings (Figure 7). Each CR can be driven independently. In case of station blackout, the control rods fall into their shut-down position by gravity. As secondary and additional shut-down system, small absorber spheres with a diameter of 1cm can fall by gravity (withheld by electrical valves) into long holes in the side reflector (Figure 8). The side reflector has a thickness of 75cm (this includes borated carbon bricks with a thickness of 5cm to protect the outer components of the reactor). The side reflector is divided into 30 azimuthal sections, each with either a CR-hole or two long holes for the SAS (hole circle diameter of 162.5cm).

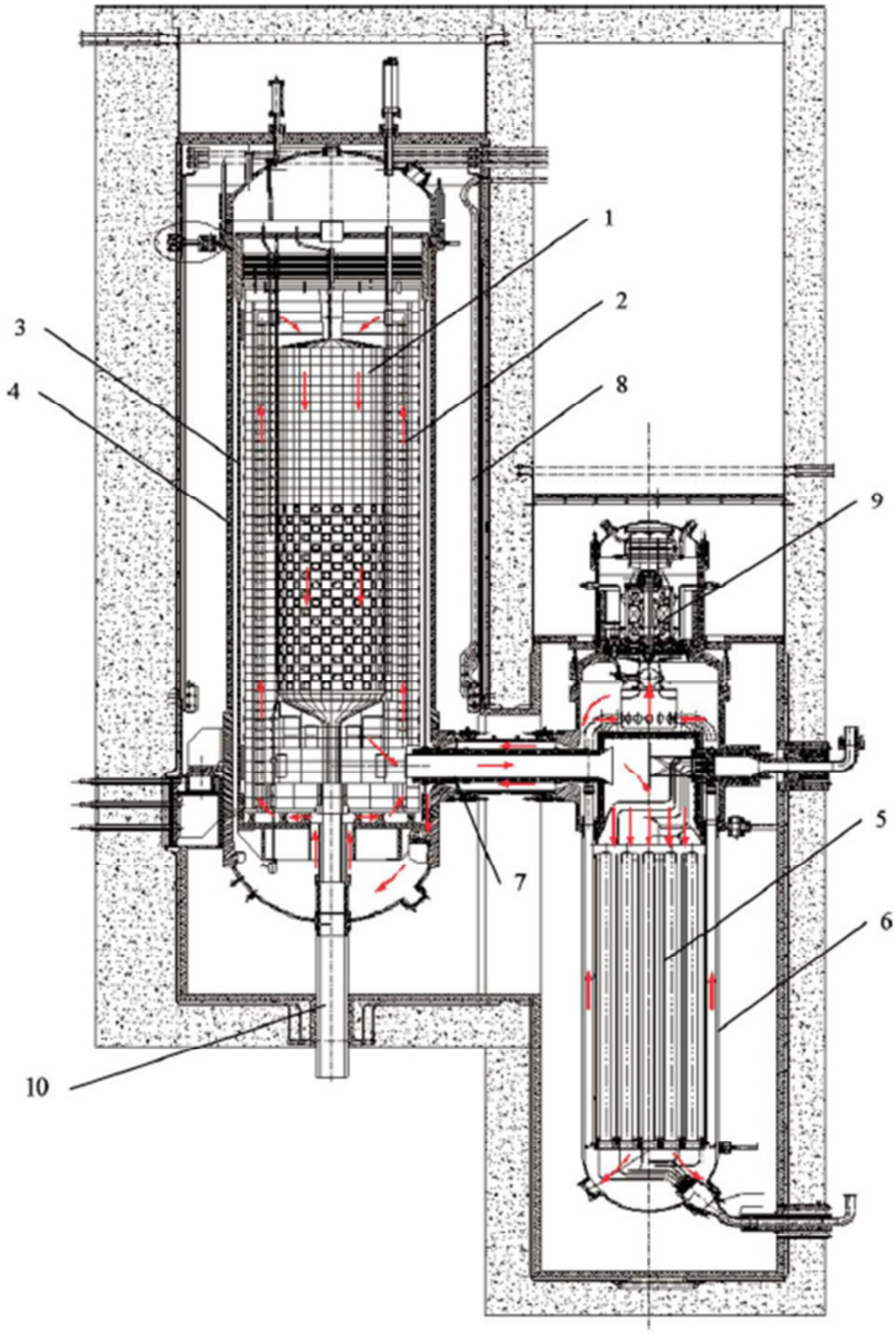

Cross-section of the HTR-PM reactor: (1) reactor core, (2) side reflector and carbon thermal shield, (3) core barrel, (4) reactor pressure vessel, (5) steam generator, (6) steam generator vessel, (7) coaxial gas duct, (8) water-cooling panel, (9) blower, (10) fuel discharging tube, (11) control rod driving system, and (12) small absorber sphere unit

Figure 5 : Cross section of HTR-PM [10]

The graphite components are kept in shape by a core barrel, which is then followed by a gaseous gap to thermally de-couple the RPV from the core barrel. The whole setup is located inside a Reactor Pressure

Vessel (RPV) made of steel. At the outside of the RPV the Reactor Cavity Cooling System (RCCS) is installed, which protects the reactor structures from temperature induced damage during accidents by transporting the expected excessive heating power to a low pressure RCCS.

The fuel of the reactor consists of fuel pebbles made of graphite, which include fuel particles with a diameter of 500µm (Figure 6). The particles have different coatings, namely a buffer graphite coating to absorb gaseous fission products, a pyrolytic carbon coating, a Silicon-Carbide coating and another pyrolytic carbon layer (TRISO). The Silicon carbide coating forms a strong barrier for diffusion of fission products and forms itself a pressure tight containment for fission products. The main fuel parameters can be found in

Table 2.

Table 1 : Main design parameters [9]

Parameter	Unit	Value
Rated electrical power	MW	110
ReactorThermal Power	MW	250
Average core power density	MW/m^3	3.22
Eletrical Efficency	%	42
Primary helium pressure	MPa	7
Helium temperature at reactor inlet/outlet	°C	250/750
Helium flow rate	kg/s	96.3
Numer of Helium riser channels	-	30
Active core diameter	m	3
Equivalent core height	m	11
Height upper void	m	0.57
Number of control rods	-	8
Diameter of control rod holes	cm	65
Number of SAS	-	2x22
Type of steam generator	-	Once through helical coil
Main steam pressure	MPa	13.24
Main steam temperature	°C	566
Main feed-water temperature	°C	205
Main steam flow rate at the inlet of turbine	t/h	673

Table 2 : Main fuel element parameters [9]

Parameter	Unit	Value
Fuel Type	-	TRISO
Heavy Metal (HM)	-	UO2
Radius of U- Kernel	µm	250

Thickness of the 4 Kernel Layers	µm	95 / 40 / 35 / 35
Density of HM-Oxide	g/cm3	10.4
Density of the 4 Coatings	g/cm3	1.05 / 1.9 / 3.18 / 1.9
Radius of Fuel Matrix	cm	2.5
Radius of Fuel Element	cm	3.0
Graphite Density of Matrix	g/cm^3	1.74
HM per fuel element	g	7
Enrichment of fresh fuel	%	8.9
Thermal absorption cross section of Graphite [Fuel and Reflector]	mbarn	4
Number of fuel elements in reactor core	-	420,000
Average burn-up	GWd/tU	90
Pebble-bed porosity	-	0.39
Fueling mode	Multipass	15

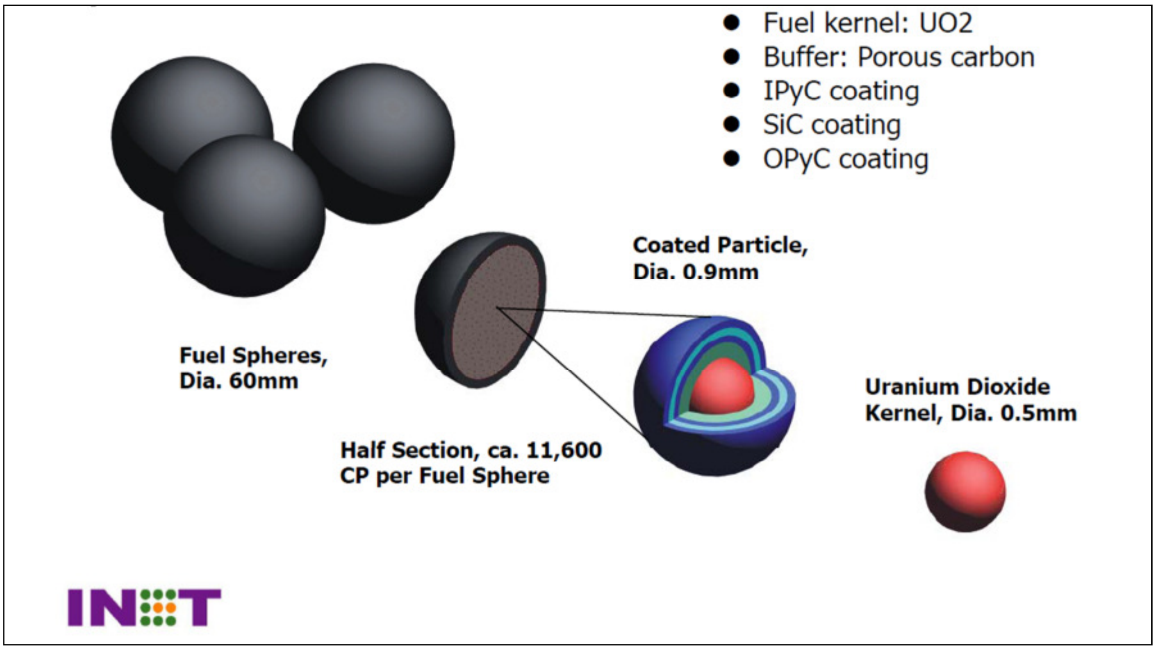

Figure 6 : Layout of fuel Elements (Source: INET)

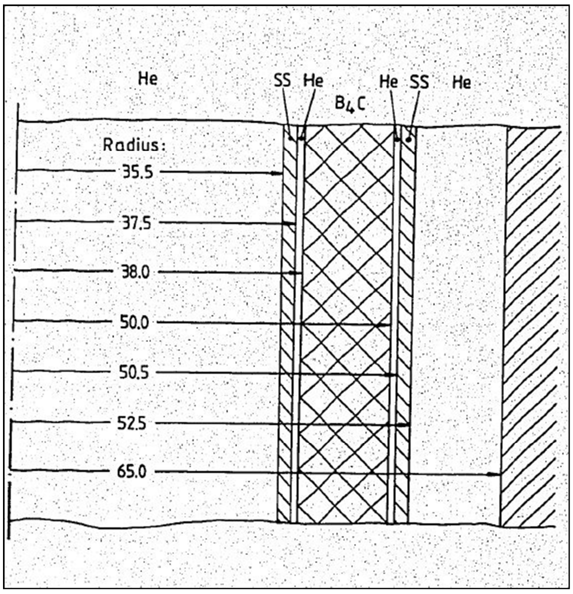

Figure 7 : Control Rod layout (SS : Stainless Steel)

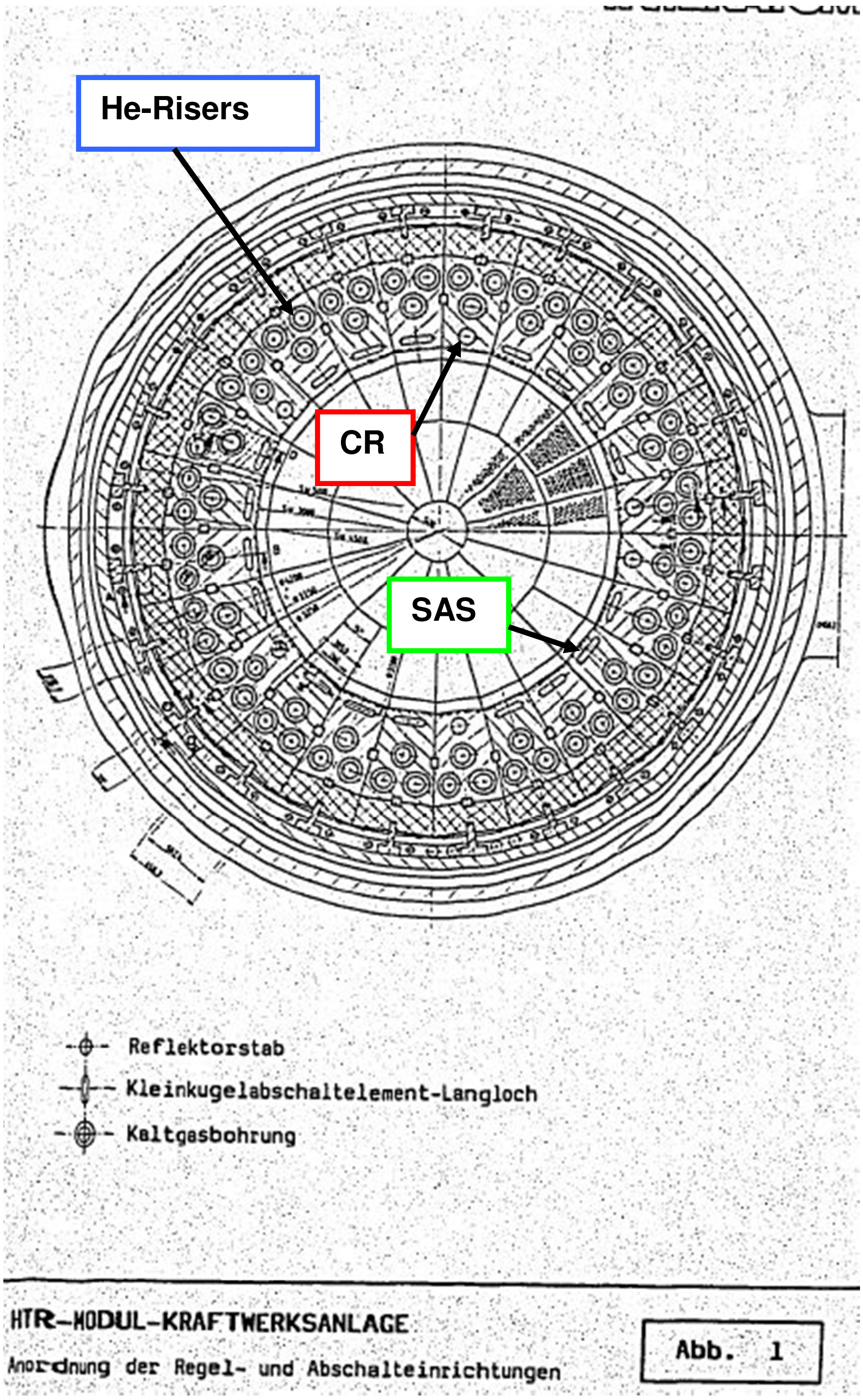

Figure 8 : Horizontal cross section of HTR-Module

3 Hot Spots and Areas

3.1 Definition and Configuration of Hot Spots and Areas

Hot spots and areas in pebble bed cores can occur as a consequence of more densified pebble clusters or of unexpected fuel loading patterns and fuel handling inside the reactor.

A variation of the flow velocity of one of the pebble flow channels mentioned above might lead to a higher or smaller burn-up of the specific zones and therefore to a more imbalanced power distribution. The highest effect is expected at the radially innermost flow channel since the highest pebble flow velocity occurs here.

Hot spots in Pebble Beds might be triggered through a densification of the fuel pebbles [11] [12]. This will lead to a reduction of coolability of the densification. A higher density of the fuel pebbles also leads to a local increase of the moderator density.

If the densification migrates through the core as part of the normal fuel cycle, the change in moderator to fuel ratio may lead to spectral changes and as a consequence, to burn-up and power density changes which could be determined.

The densification might also occur spontaneous during normal operations, which leads to a cluster of pebbles with an unaffected nuclide vector of previous burn-up.

The consequences of these considerations during accident conditions have also to be determined.

The effects described above can also occur for a cluster of fresh fuel pebbles.

3.2 Definition of Evaluation Cases

One working point would be the modification of the flow channel velocity. A variation of +-20% of the velocity during normal steady state will be accomplished and compared to the previous steady state.

Another study will be the influence of a wrong fuel loading pattern. It will be assumed that, after the run-in phase to the equilibrium core, only fresh fuel pebbles will be loaded to a pebble flow channel. The effect is expected to be greatest at the innermost flow channel resulting from the highest neutron flux. A test case loading fresh fuel in the innermost zone will be investigated and compared to the previous steady state results.

For the following considerations for the TORT-TD/ATTICA^{3D}, it is assumed that the densification occurs after the run-in phase of the core.

A small zone with a modified cross section set is to be defined with the following modifications:

The densification forms an area with a smaller porosity, additional influence may be the fuel loading pattern where a series of fresh fuel is introduced into the core and forms a densification.

Stationary results are to be achieved for the following different cases:

- Densification in the maximum of neutron flux
- Densification in the maximum of neutron flux with a bulk of fresh loaded fuel elements
- Densification at the temperature maximum (near the lower end of the core)
- Densification at the temperature maximum (near the lower end of the core) flux with a bulk of fresh loaded fuel elements

To gather reference information about local densifications, MCNP calculations will investigate the influence of the lower porosity of the pebble bed as a reference for the following simulations. The MCNP calculations will be done without consideration of burn-up. The results will be compared to the normal pebble bed results.

Transient calculations are intended for the following cases:

- Control rod ejection: The ejection of one control rod leads to a power excursion. The influence on temperature and power distribution will be investigated.
- PLOFCA (pressurized loss of forced cooling accident): The influence on temperature will be investigated.

- DLOFCA (depressurized loss of forced cooling accident): The influence on temperature will be investigated.

With the transport code MCNP, it is possible to simulate every single fuel particle inside the pebble. In this example, the distribution of the fuel particles are achieved by using a regular lattice of cubes, each consisting of the fuel particle with a diameter of 500 µm and a surrounding mixture of fuel matrix graphite with the coating materials (Figure 9). The MCNP built-in uranium card can provide additional information by randomly distributing the fuel particles inside the graphite matrix.

It is foreseen to do MCNP calculations with some fuel pebbles in different configurations, thereby simulating different porosities of the pebble bed. Fuel compositions of the equilibrium core will be will be used as starting point. The calculations results are intended to be used as reference for the influence on neutron flux of the densification for the following TORT-TD/ATTICA^{3D} calculations.

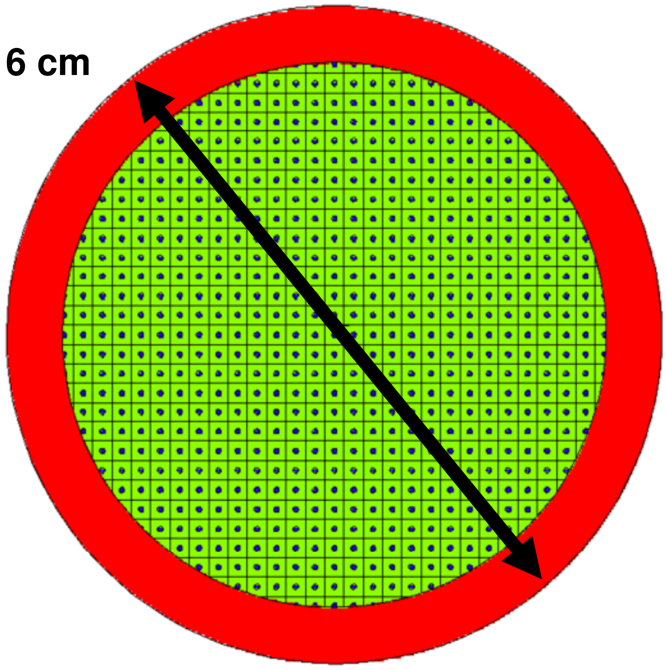

Figure 9 : Representation of a fuel pebble in MCNP

For pre-processing, a ZIRKUS calculation of the HTR-PM layout is performed to achieve the nuclide densities and cross sections of the equilibrium state. For this purpose, the core is divided into 8 flow zones of equal area (and therefore volume) to model the pebble flow adequately, see Figure 10. For every reload interval the fuel shuffling and re-loading module of ZIRKUS takes the determined nuclide densities and transfers them to the next lower core zone. Due to the different number of axial subdivision, real pebble flow behaviour can be accounted for, i.e. pebbles flow like sand in an hour-glass. From earlier experiments for pebble flow it was concluded that the innermost channels are 1.5 times faster than the outermost flow channel. This explains the number of subdivisions to be 16 for the innermost and 24 for the outermost channel. When preparing the macroscopic parameterised cross sections for the coupled transient calculation (especially for a rod ejection), the geometry necessary for pebble refuelling and shuffling can be simplified and the number of compositions within the geometry is reduced. For the starting point of the equilibrium core, the HTR-PM was simulated with 13 neutron groups and 399 material compositions. With the adequate condensation and averaging tools of ZIRKUS, the 13 neutron groups were condensated to 7 neutron groups. Also the 399 material zones including flow lines are averaged volumetrically to a 234 material zone map, see Figure 11.

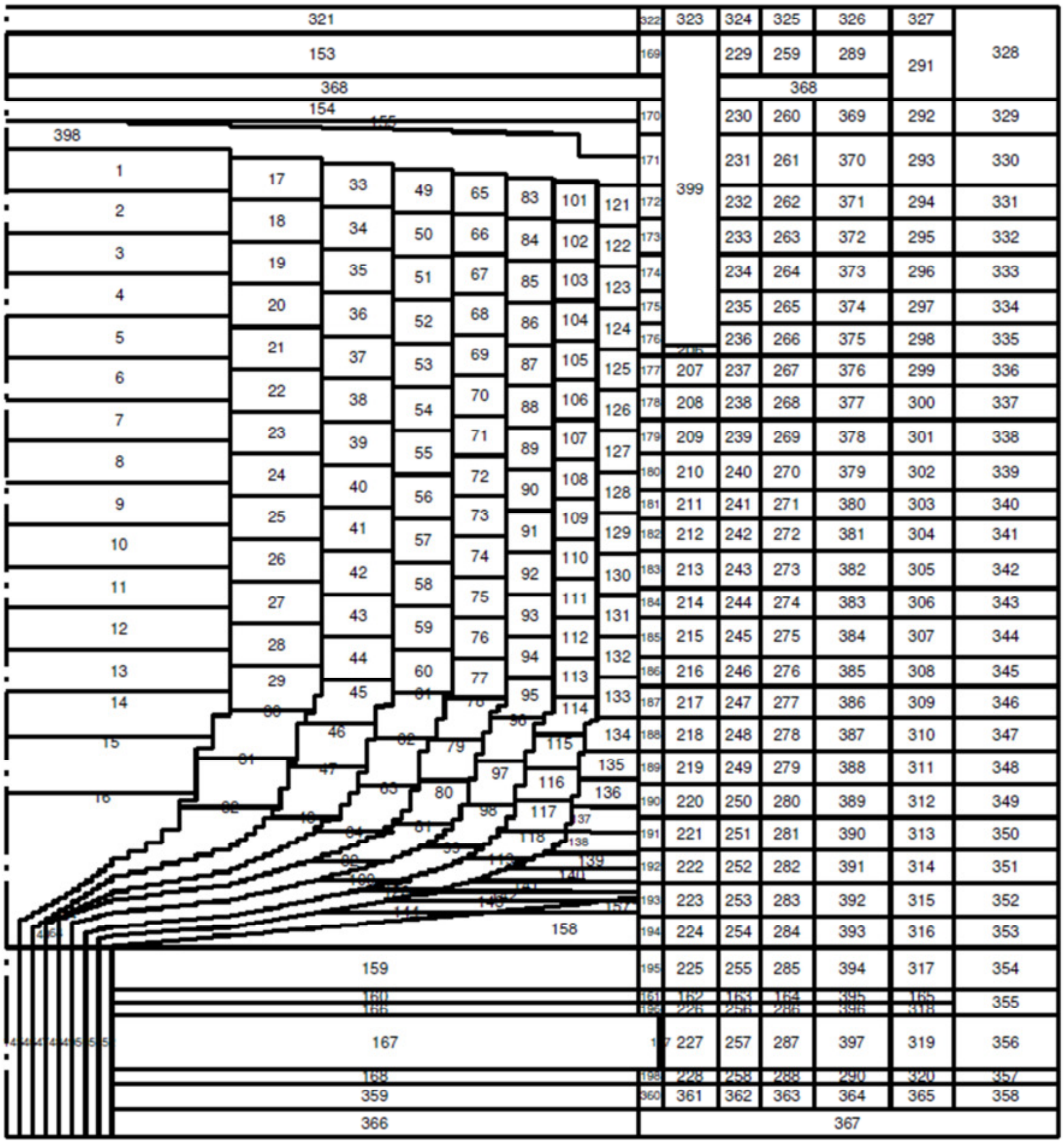

Figure 10 : HTR-PM geometry with pebble flow channels modelled according to experimental findings of pebble flow

The control rods are modelled as a grey curtain to achieve a critical reactor (Figure 11, zone 199). The reflectors and other core structures are divided into different zones to provide detailed consideration of thermal and material for the cross sections. Different pebble flow velocities and their influence can be investigated with analysis of ZIRKUS results. It will be assumed that the densification occurs after the formation of the equilibrium state of the core.

Since ZIRKUS is a 2D-code, the cross sections represent a 2D reactor model. Therefore, only densifications on the symmetry axis can be correctly simulated by ZIRKUS. The densification leads also to a decrease of pebbles in the surrounding channel areas. Since it is assumed that the pebbles move in flow channels, the decrease is only expected to occur in the flow channel cells above or below the densification. The unintended loading of fresh fuel can also be simulated.

Figure 11 : Representation of neutronic zones in ZIRKUS after condensation from 13 to 7 neutron groups. TORT-TD uses this material composition map

For the calculation in TORT-TD/ATTICA^{3D}, the generated cross sections from ZIRKUS are used. Figure 12 and Figure 13 show a 180° representation of the HTR-PM in ATTICA^{3D}.

The neutronics discretisation model of TOR-TD is similar with the ZIRKUS model, but expanded azimuthally to 180° into 13 zones, also representing the control rods. The ATTICA^{3D}-model is divided into similar azimuthal zones. The control rods can be driven individually by TORT-TD input options. The flux and spectra are calculated by TORT-TD model. The zonal structure in the densification is more resolved than adjacent regions to gather the desired information.

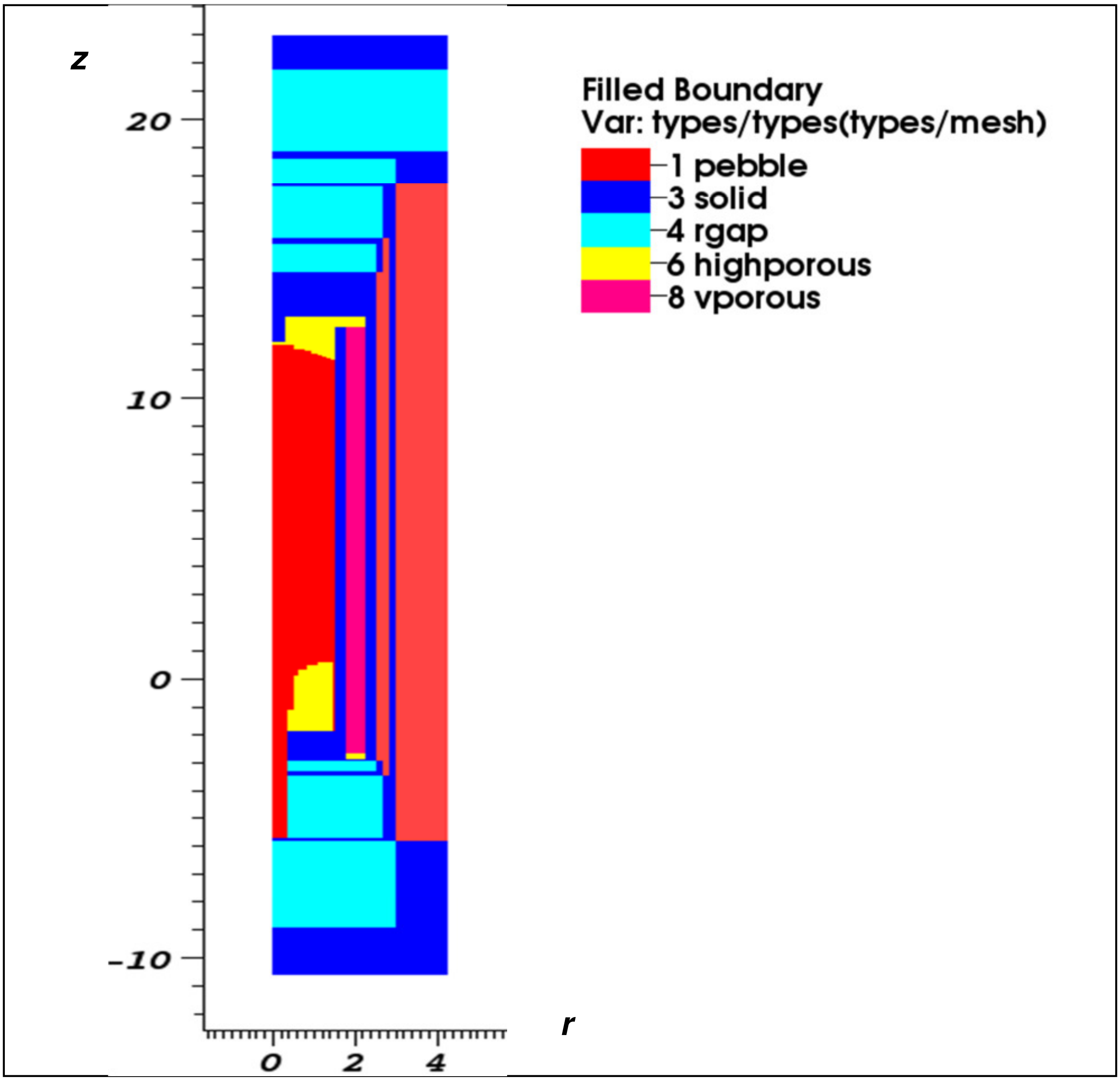

Figure 12 : Cross section of representation of thermal hydraulic zones in ATTICA^{3D}

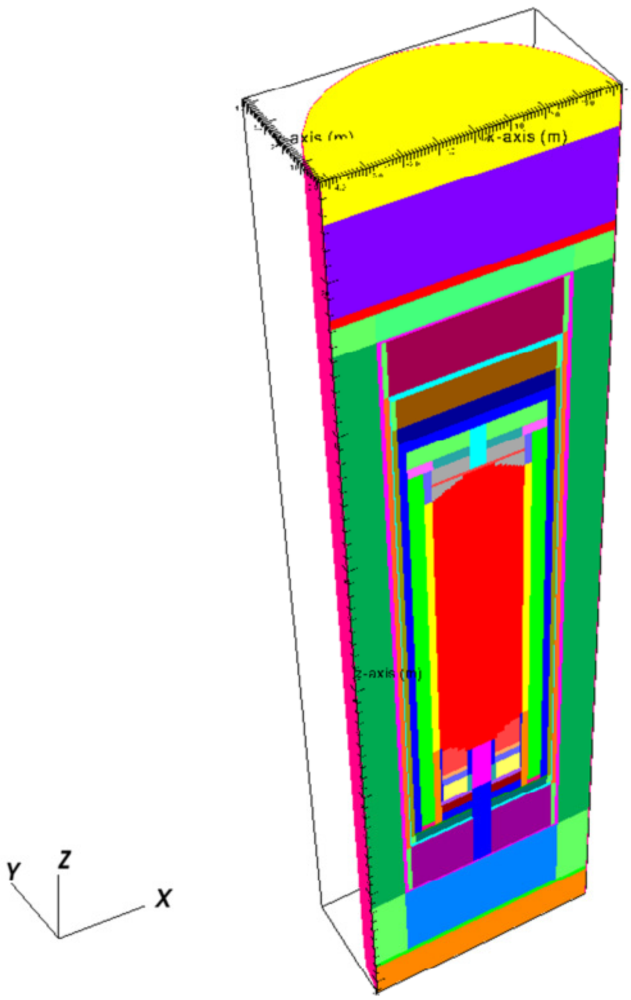

Figure 13 : 180° ATTICA^{3D} model with components

3.2.1 Modeling of densifications

The densification in the pebble bed is modelled according to the results of Auwerda [13]. Auwerda specifies a number of around 45 pebbles for the size of one densification cluster. The radius is determined by the cubic root of 45, resulting in around 3.5 pebbles per cube. This results in a diameter for a certain cylindrical densification of almost 20 cm. For the densification cluster, the cross sections must be modified, because in ZIRKUS only the global porosity of the densification cluster can be determined. As the cross section must be specified for each zone in the model, a zone with a height of 70 cm is produced for the densification cluster. Figure 14 shows the porosity over the radius.

Under the assumption that the pebble loading of the reactor operates correctly, meaning that the pebble flow is not interrupted, a more porous region above the densified zone is assumed. Furthermore it is assumed that the densification is formed during normal operation. Therefore there is no influence of the depletion to be expected within the pebbles and their nuclide compositions. So the corresponding cross sections are modified according to the change of porosities.

As a filling factor for the densification, a maximum 0.71 was estimated by Auwerda; for the less densified zone above the densification, a filling factor of 0.58 is assumed.

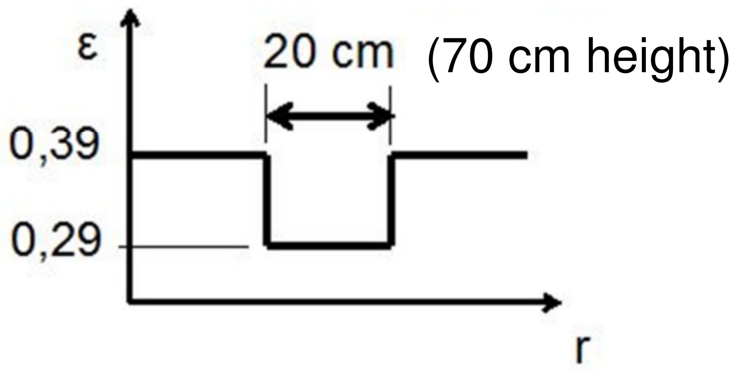

Figure 14 : schematics of the porosity change

The modification of the cross section can be derived from the following equation:

$$N_T = \frac{A}{M}\rho \tag{1}$$

The effective density in a mesh, as well as in the pebble bed, depends on the porosity:

$$\rho_{eff} = \varepsilon\rho \tag{2}$$

Here M denotes the molar mass and A mass number. The macroscopic cross section Σ is proportional to nuclide density. The ratio of A/M is constant. It can be concluded:

$$\Sigma = \frac{A}{M}\cdot\rho_{eff}\cdot\sigma \tag{3}$$

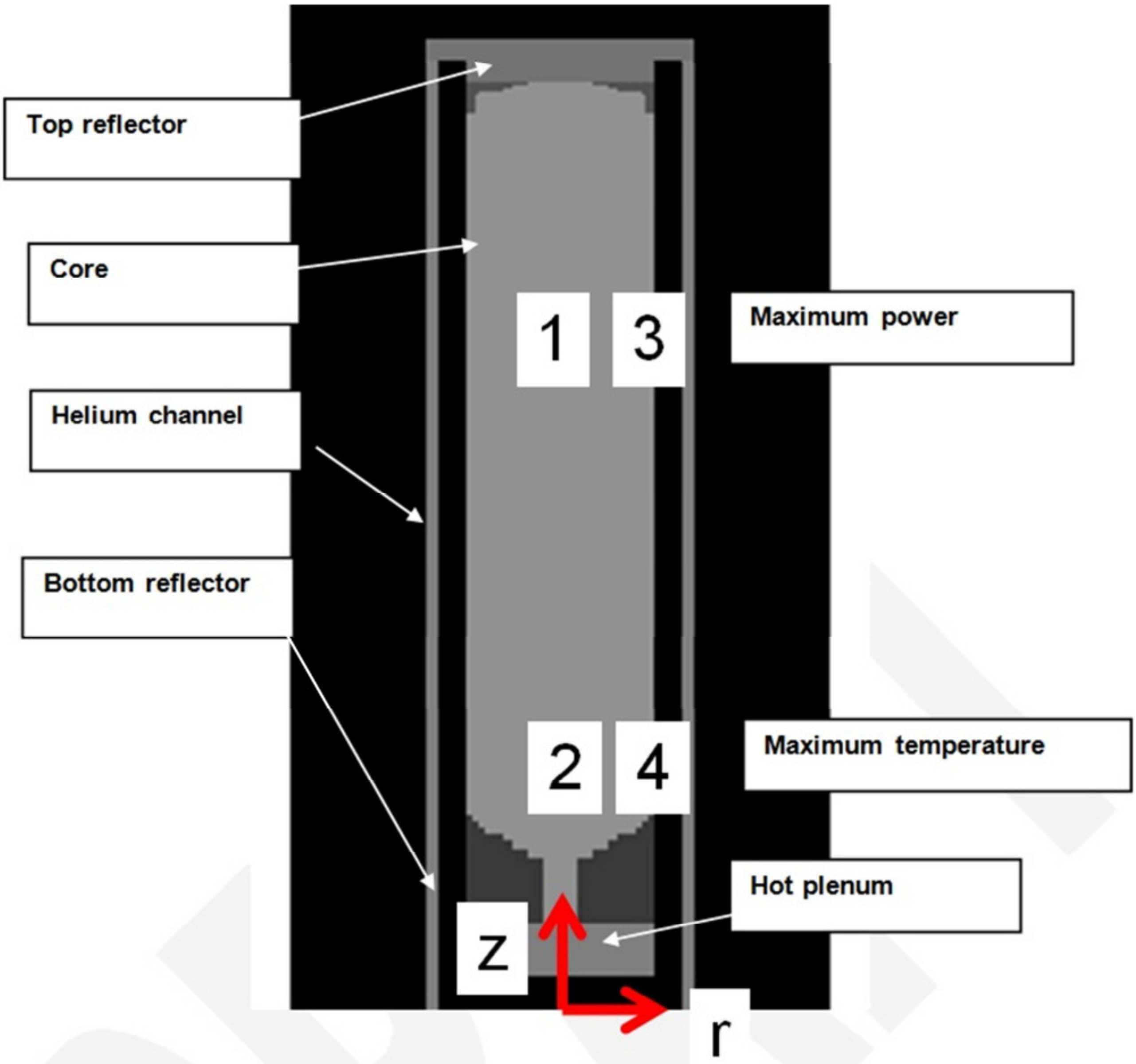

Figure 15 : Location of the densifications

By decreasing the porosity, the nuclide density increases to the same extent and, hence, also the cross sections will change. The moderation ratio, the ratio of the nuclide density of moderator over fuel, remains the same. Under the assumption that the influence of the neutron spectrum in the densification cluster is of minor importance, the corresponding cross section can be modified according to the porosity. A densification with a porosity of 0.29 - in comparison to the normal 0.39 - produces a power factor of 1.168 for the densified region; and 0.951for the less dense region (porosity 0.42). This factor will be used to modify the cross sections for the regions of interest.

For this investigation, the porosity change is carried out in different selected positions in the pebble bed: one in the region with the maximum power, at the symmetry axis and at the edge of the pebble bed, another in the region with the maximum gas temperature at the bottom of the pebble bed, also at the symmetry axis and the edge of the pebble bed.

Table 3 : Location of densifications

	Symmetry axis	Outer channel
Power maximum	1	3
Lower core	2	4
Geometry	Cylinder on centreline	Annular segment

Table 4 : Position of densifications

Case	Height [cm]	Radius [cm]	Angle [°]
1	1034,1 - 1100,1	0 - 10,94	0 - 180
2	1034,1 - 1100,1	129,90 bis 140,31	0 - 7,66
3	351,1 - 431,1	0 - 10,94	0 - 180
4	351,1 - 431,1	129,90 - 140,31	0 - 7,66

The positions of the densification clusters are represented in Figure 15. The densified regions in the symmetric axis are of cylindrical shape, the densification at the edge change is a fraction of an annulus. Therefore the angle is calculated as consequence of the volume unit with cylindrical form. As inner and outer radius the radii of the TORT-TD geometry will be used (Table 3, Table 4). The angle of the outer densification is calculated as 15.31, for a 180°. For symmetry reasons, the densification of the simulation is only half the angle.

The ATTICA^{3D}-model consists of 17 angles with 5 control rods. With 75 z-meshes and 33 radial meshes, there are 42,705 meshes for the ATTICA-model (Figure 16). The whole height of the model is 30.957 m with a 4.26 m radius. As boundary condition a constant heat transfer over the edge of the cylinder is modeled. The cooling gas flows enters with an initial temperature of 523 K and a flow of 96 kg s^{-1}. The heterogeneous temperature model is used with an outer free-fuel zone and 5 subdivisions for the fuel zone.

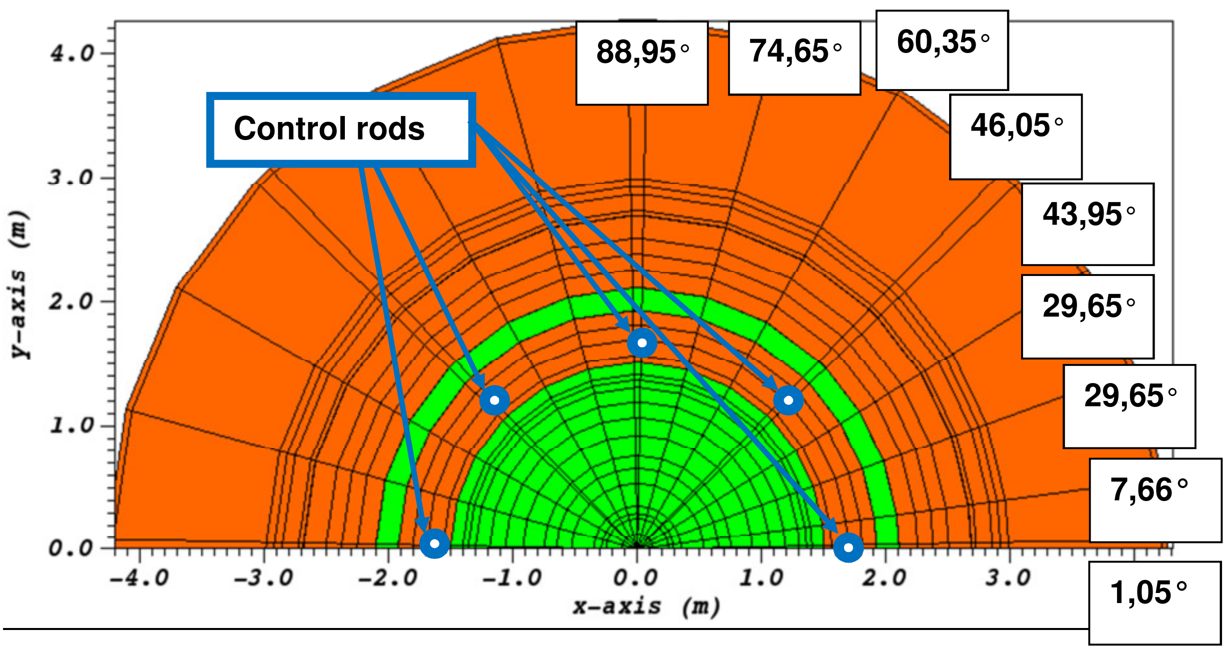

Figure 16 : Horizontal section with 180 ATTICA-model HTR-PM (orange: no flow, green: flow path)

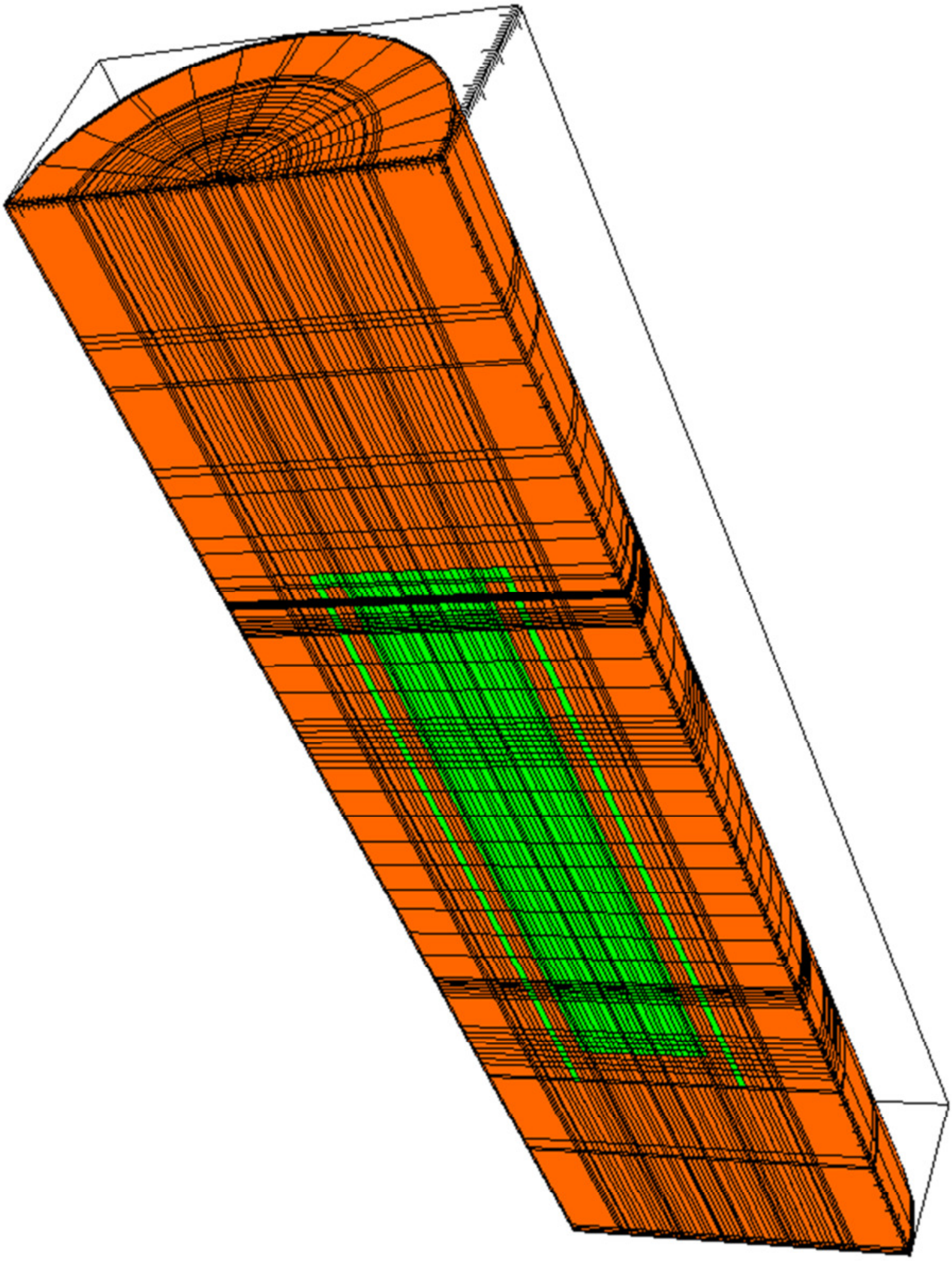

Figure 17 : 180° ATTICA^{3D}-model (orange:no flow, green: flow path)

3.2.2 Depressurised loss of forced cooling accident with densifications

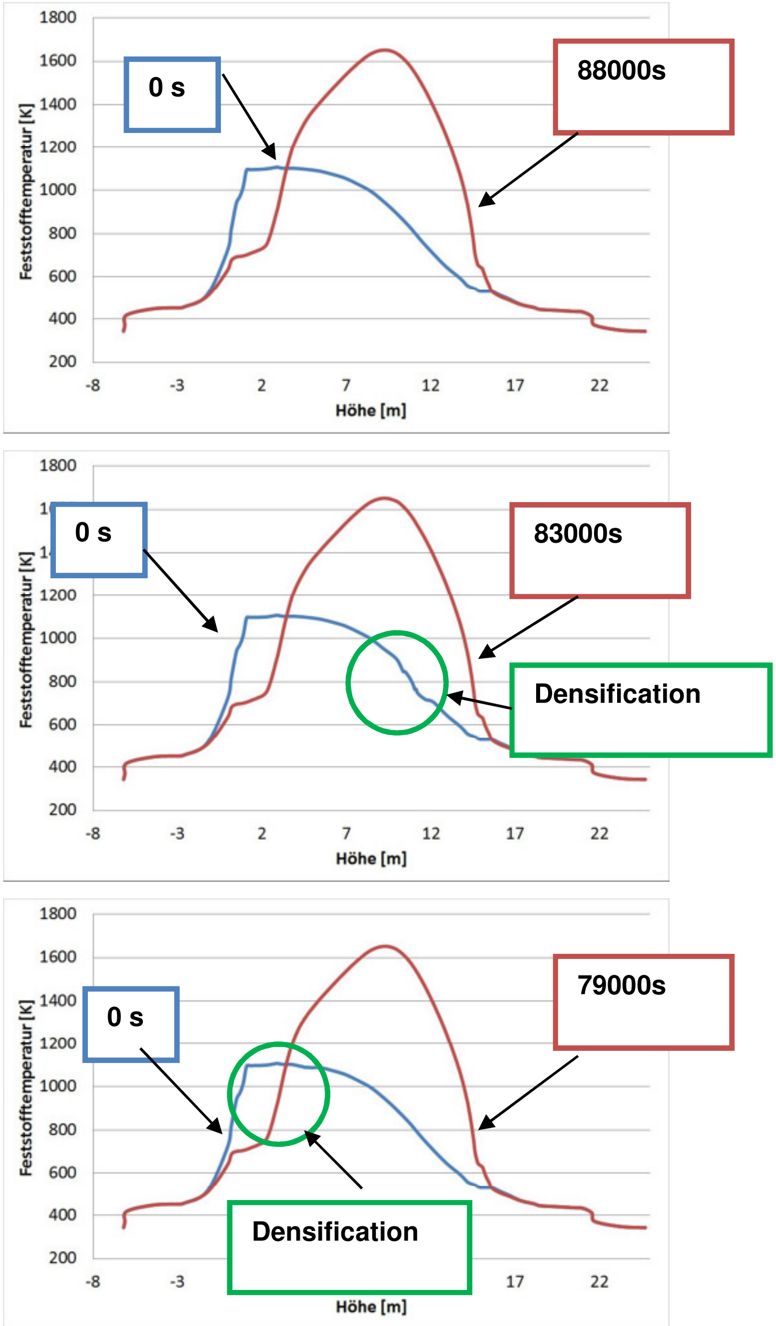

Figure 18 : DLOCA at the HTR-PM, maximum temperatures at the symmetry axis: 1) without densification, 2) with a densification at z = 10 m, 3) with a densification at z = 1m

A DLOFCA is simulated to analyse the influence of the densification. An instantaneous pressure relief to atmospheric pressure is assumed as well as a reactor shutdown, so just the remaining decay heat must be carried out of the system.

To simulate this case faster, an implemented ATTICA^{3D} function was used. For the DLOFCA approach, it is assumed that the coolant has no significant impact in the heat transport at atmospheric pressure and therefore the coolant's impact is not calculated which can be regarded conservative. For the simulation, the decay heat is computed according to DIN 25485. The power distribution is taken from the previous ZIRKUS calculations, for the densification cluster and the less dense cluster the power is partially modified according to the porosity change. A coupling with neutronics is not performed.

For the densification on the symmetry axis, the problem reduces to a quasi-2D (one azimuth) 30-model of the HTR-PM.

Figure 18 shows the temperatures at the centreline of the ATTICA^{3D}-model. Small deformations can be seen at 0 s in the densification cluster, apparently it can be transported with the coolant leading to temperatures increase of only 10 K.

3.2.3 Asymmetrical ejection of rods with densification

The data for the modified cross sections of the densification cluster and the control rods were used for the control rods ejection simulation. The transient is based on the OECD/NEA-Benchmark for the PBMR [15], this means that the complete control rod ejection out of the reactor occurs in 0.1 s. resulting in a rod velocity of 46 m/s. The complete simulation time of the transient is 50 seconds. Only 3 control rods are ejected.

Figure 19 shows the flow within and around the densification cluster. The reduced flow velocity is obvious. In addition, the coolant avoids the densification cluster. With helium the heat transfer coefficient increases with increasing temperatures, also in the graphite. Hence, the effective heat transfer capacity in the zone increases such that power increase can be compensated by adjacent zones and the surrounding gas (Figure 20).

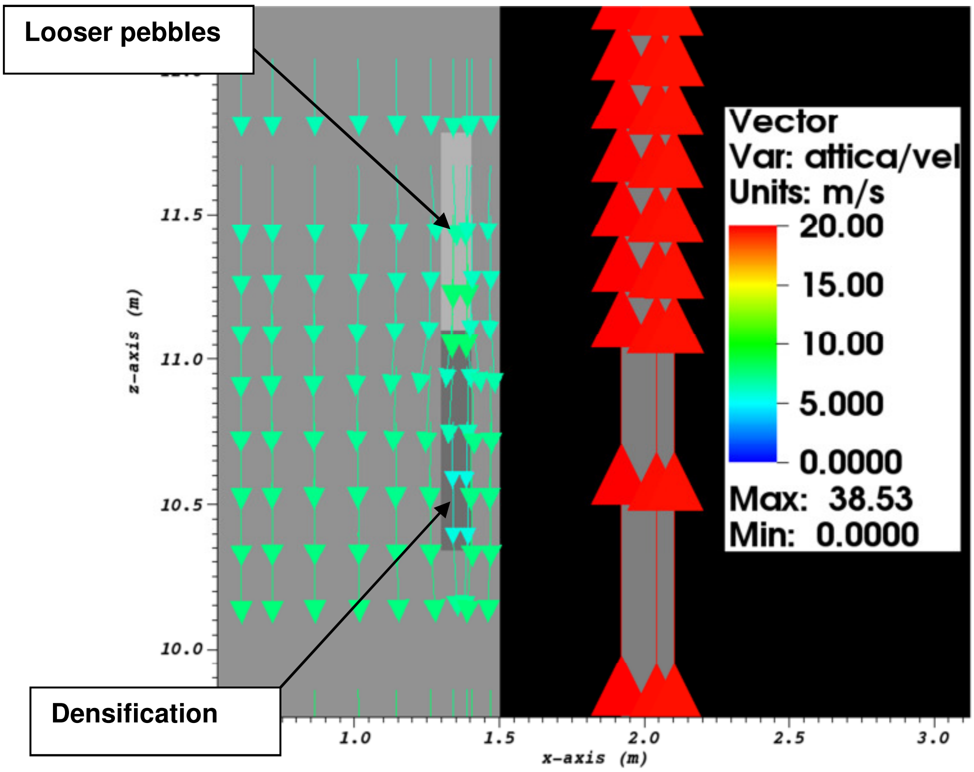

Figure 19 : Flow ratio in the densification cluster (at the maximum power height, edge region) at 0s.

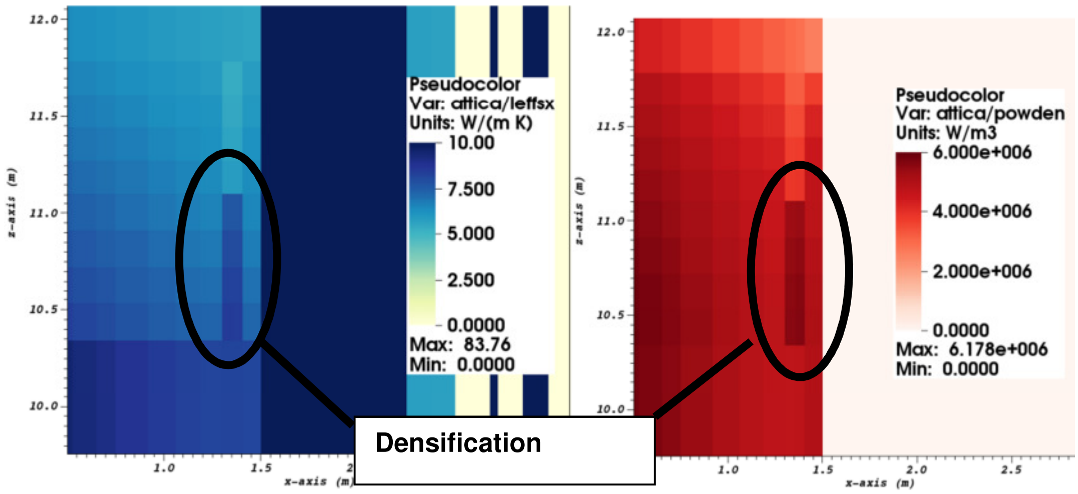

Figure 20 : effective heat transfer capacity of solid material in radial direction (left) and power density (right) in the densification cluster (at maximum power height, edge region) at 0s

The different densification scenarios are simulated for the 3-rod ejection. The power densities as well as the maximum fuel temperature are shown and discussed.

At first, the transient without densification is computed (Figure 21, Figure 22). The deformation of the power distribution as a consequence of the asymmetric control rod ejection is clearly visible, also the asymmetric temperature distribution. The maximum power is reached after 3.75 s, then, the fuel temperature coefficient counter-acts and the power reduces again. As the power is still elevated, the temperature increases and is still increasing after the final simulation time of 50 s. however the temperature increase in the fuel is in the range of 30 K.

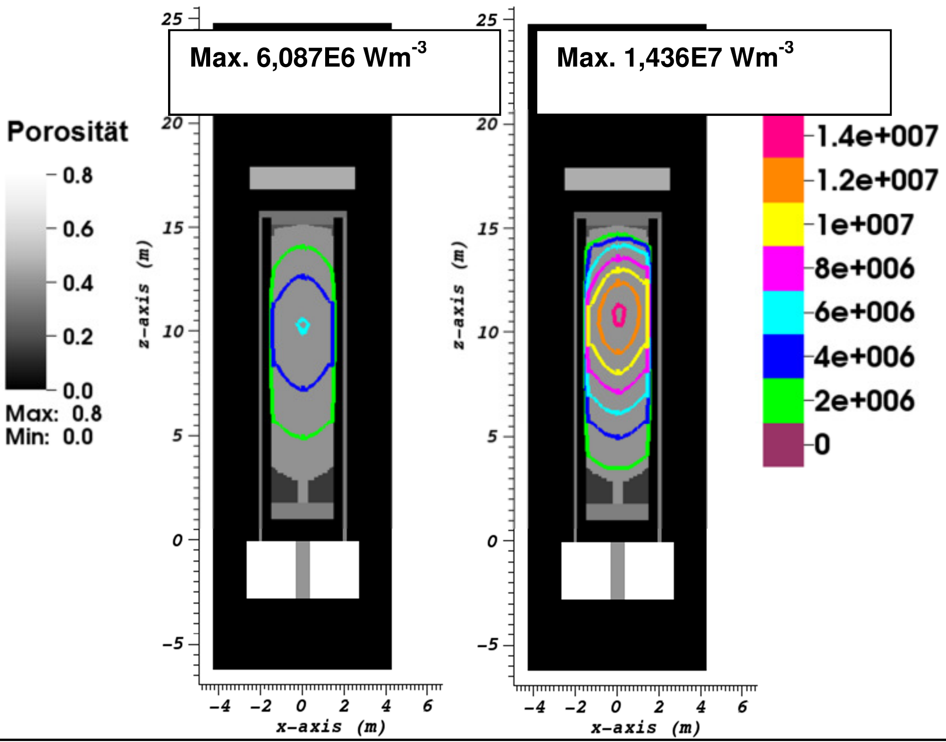

Figure 21 : Power distribution at the beginning (0s, left) and at the maximum power achieved at 3.75 s (right) for a one side control rod ejection, without densification.

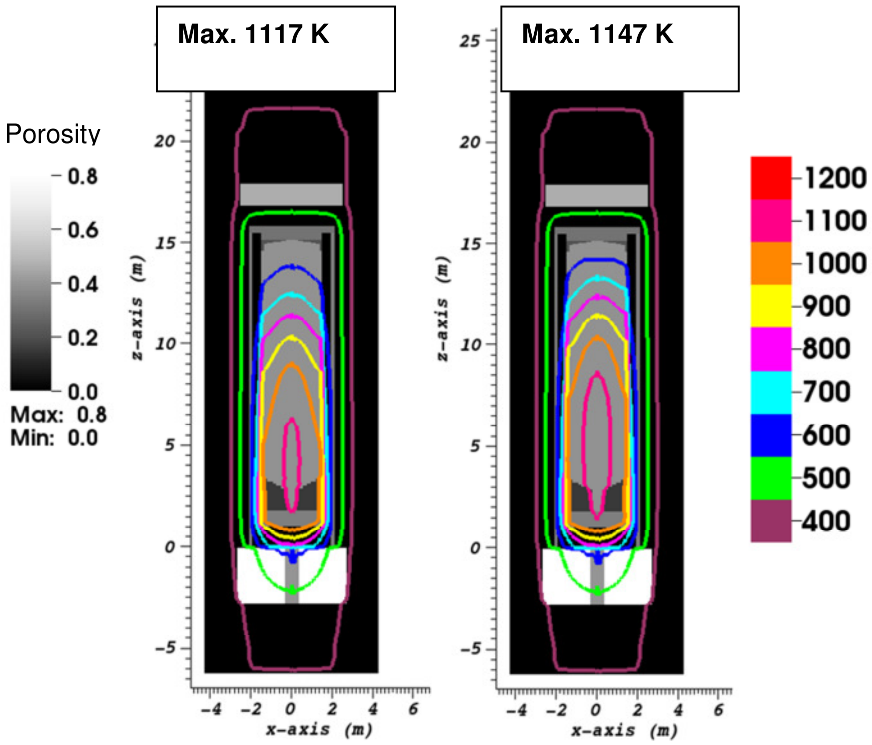

Figure 22 : Maximum fuel temperature distribution at the beginning (0 s, left) and at the end (45 s, right) of the transient for a one side control rod ejection, without densification.

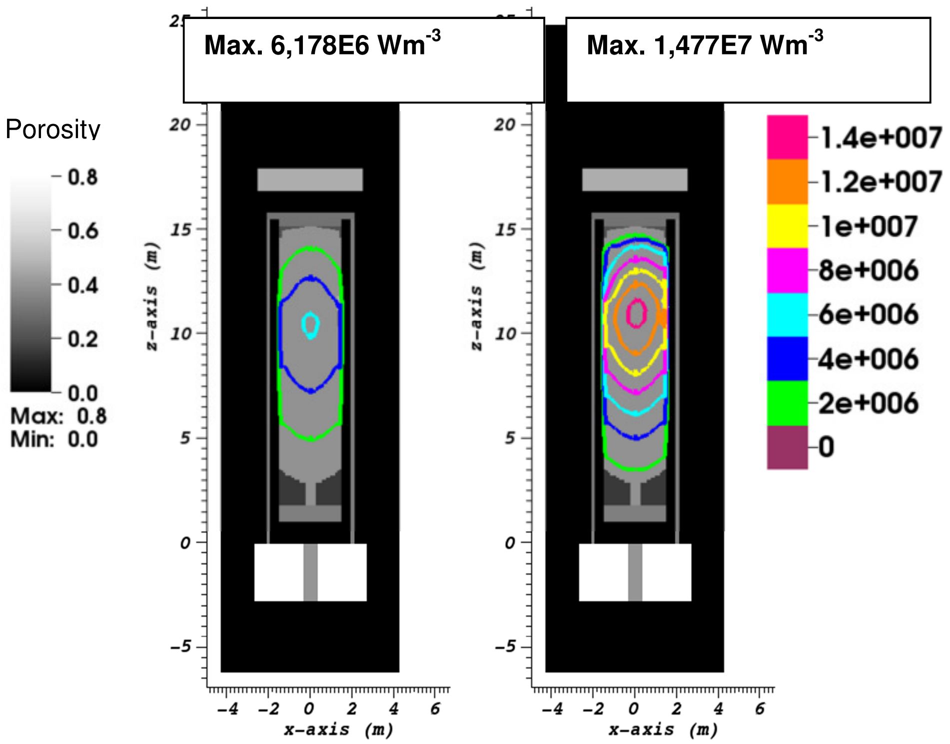

Figure 23 : Power distribution at the beginning (0s, left) and at the maximum power achieved at 3.75 s (right) for a one side control rod ejection, densification at the maximum power height, edge region

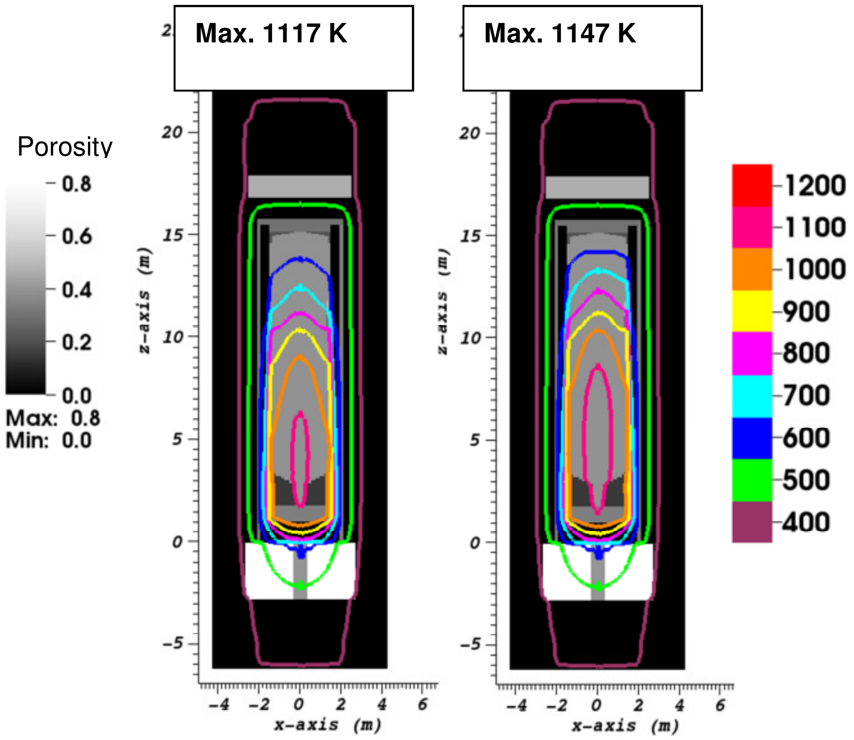

Figure 24 : Maximum fuel temperature distribution at the beginning (0 s, left) and at the end of the transient at 45 s (right) for a one side control rod ejection, densification at the maximum power height.

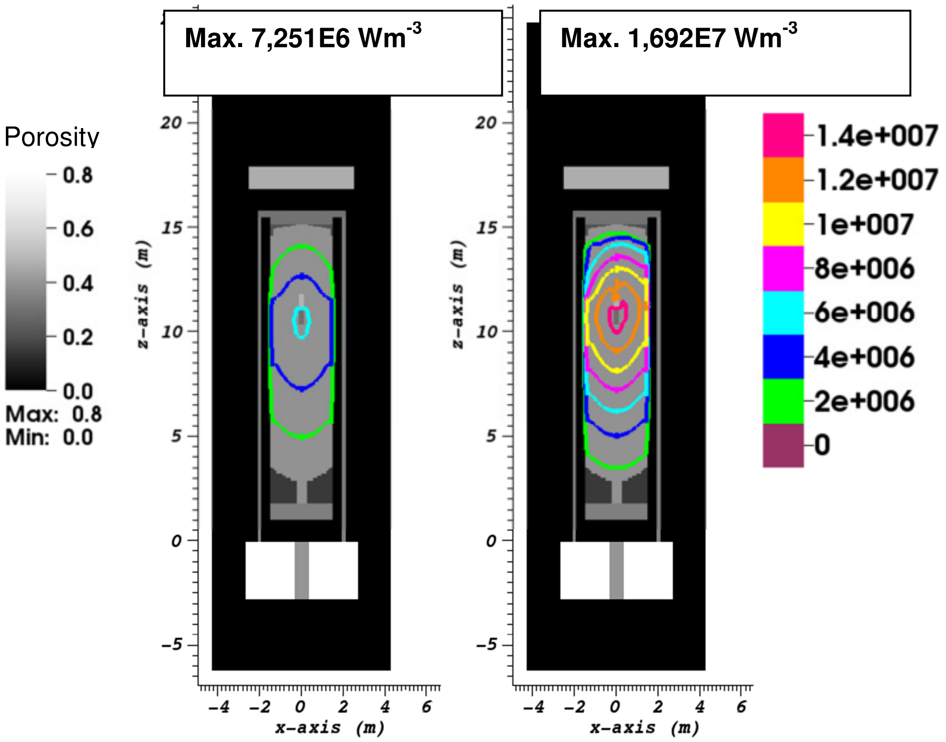

Figure 25:power distribution at the beginning (0 s, left) and at maximum power (3.75 s, right) for a one side control rod ejection, densification at the maximum power height, middle.

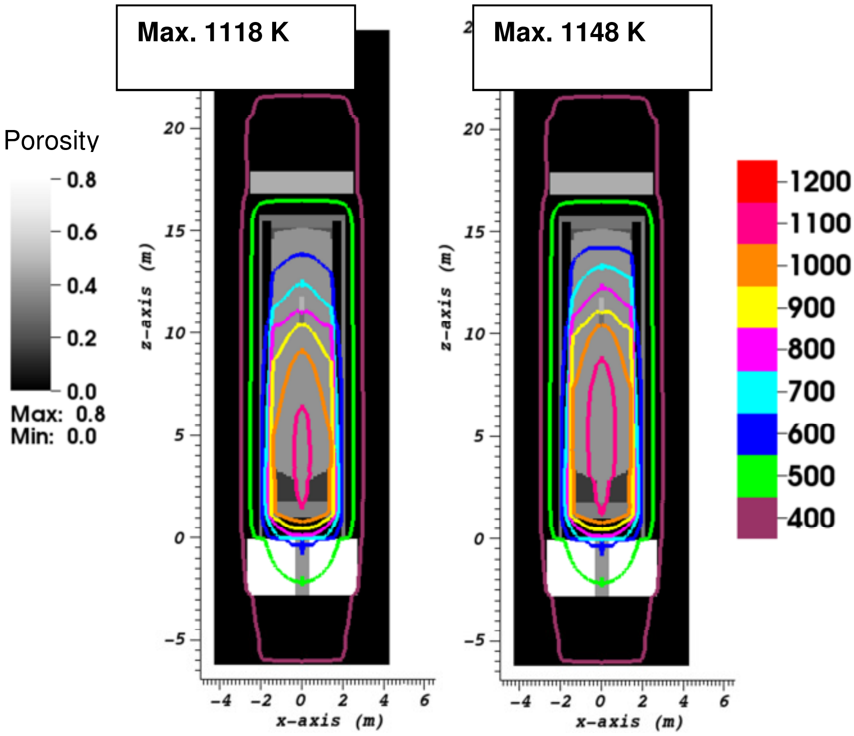

Figure 26:Maximum fuel temperature at the beginning (0 s, left) and at the end of the transient (44 s, right) for a one side control rod ejection, densification at the maximum power height, middle.

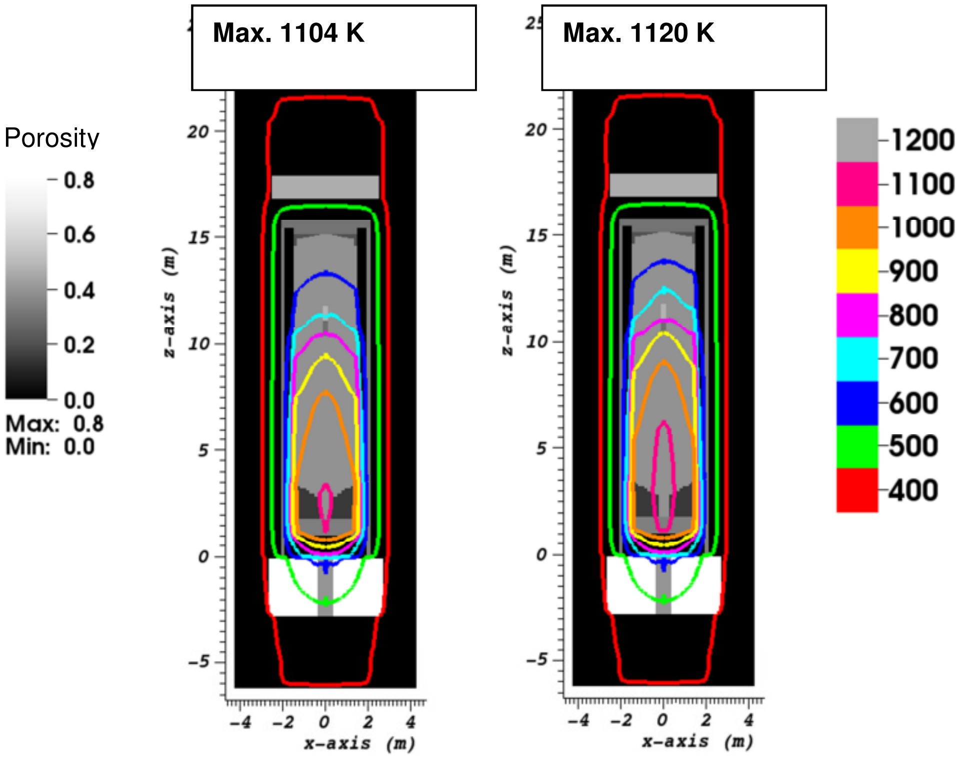

Figure 27: Gas temperature distribution at maximum power (3.75 s, left) and at the end of the transient (44 s, right) for a one side control rod ejection, densification at the maximum power height, middle.

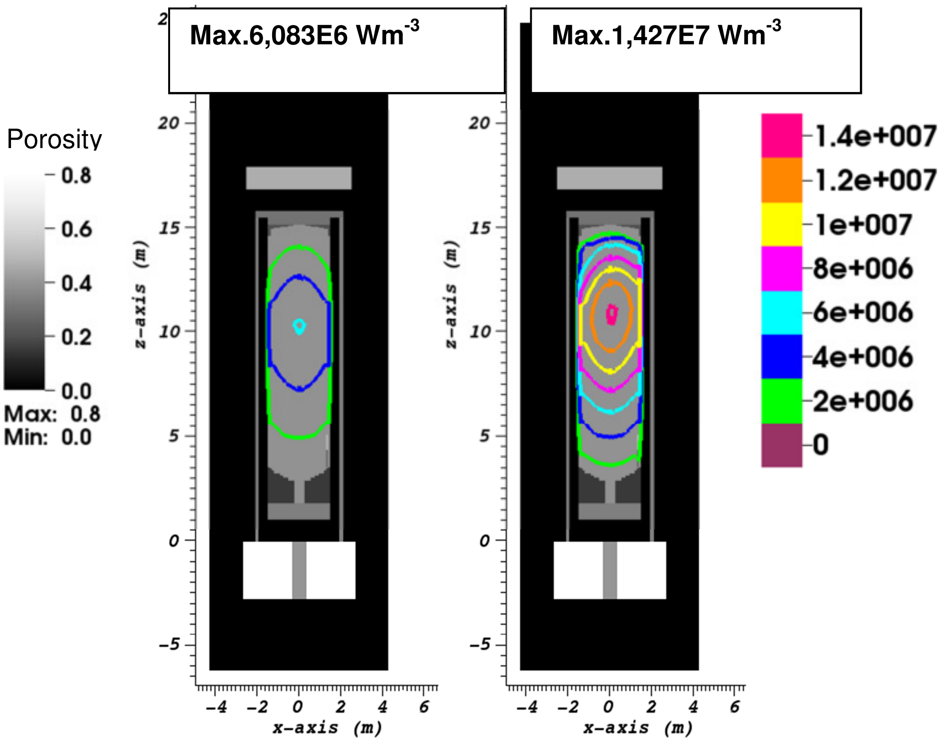

Figure 28:Power distribution at the beginning (0 s, left) and at the maximum power (3.75 s, right) for a one side control rod ejection, densification close to the bottom, edge region.

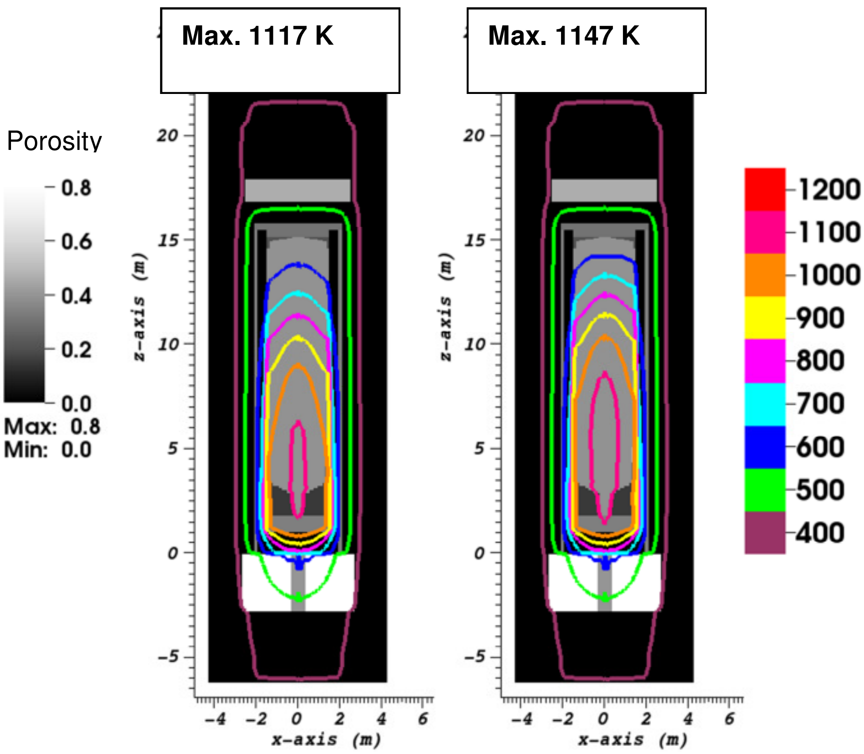

Figure 29 : Maximum fuel temperature distribution at the beginning (0 s, left) and at the end (45 s, right) of the transient for a one side control rod ejection, densification close to the bottom, edge region.

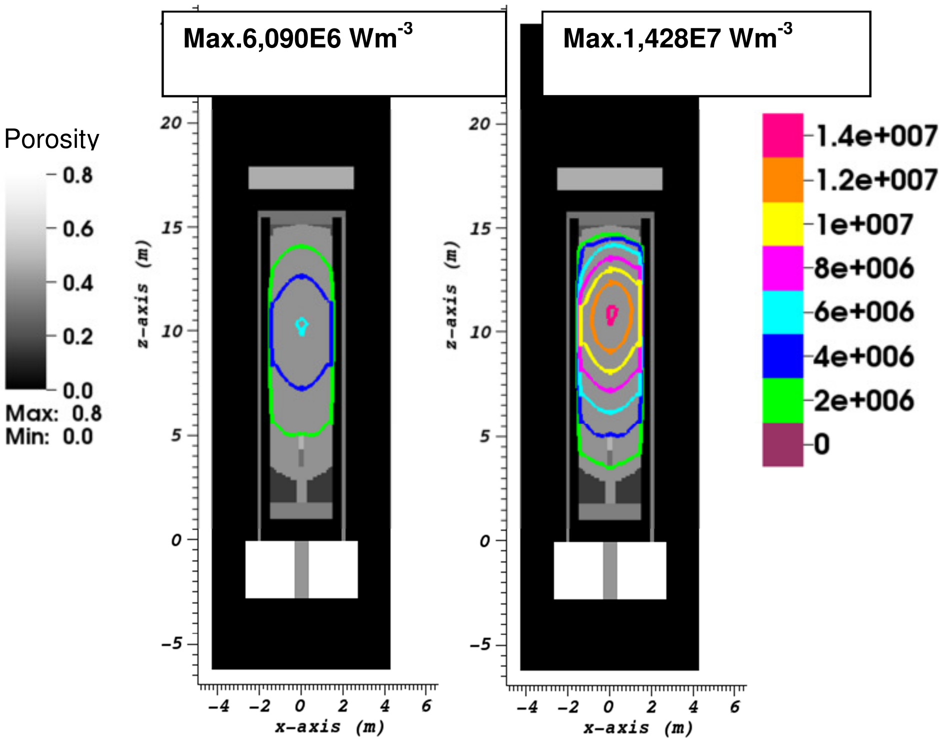

Figure 30: Power distribution at the beginning (0 s, left) and at the maximum power time (3.75 s, right) for a one side control rod ejection, densification close to the bottom, middle.

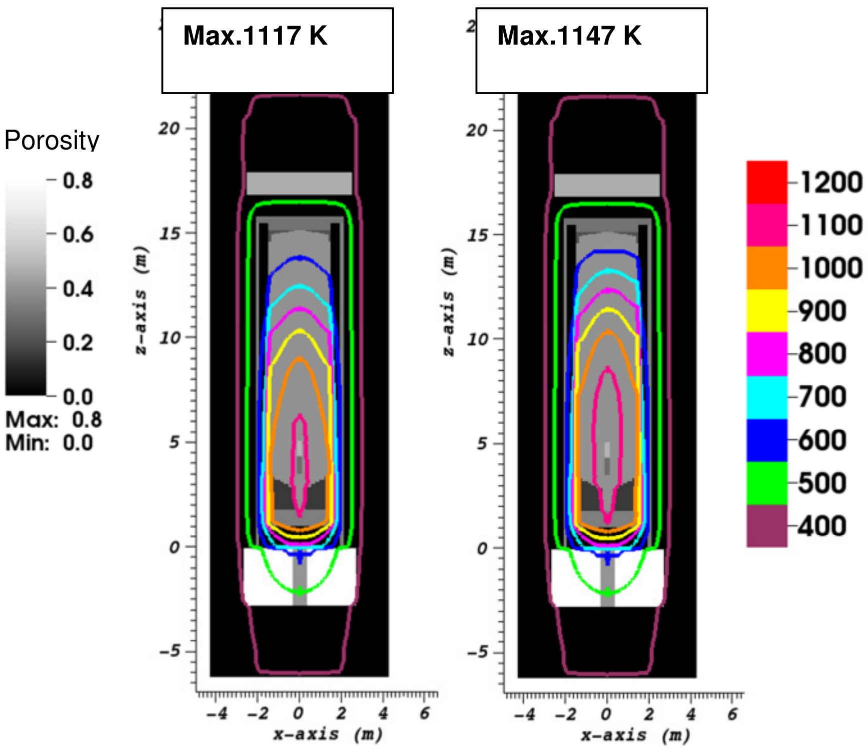

Figure 31 : Maximum fuel temperature distribution at the beginning (0 s, left) and at the end (45 s, right) of the transient for a one side control rod ejection, densification close to the bottom, middle

For the densification in case 3, the power is shifted towards the densification cluster, however the maximum power is not as big as in case 1. But the increase in the maximum fuel temperature is minimal. In case 2 and

4 the fuel temperature increases stronger as in cases 1 and 2, because here the fuel is heated by the down-coming gas from the top. The maximum power is not as high as in cases 1 and 3 and occurs also at 3.75 s.

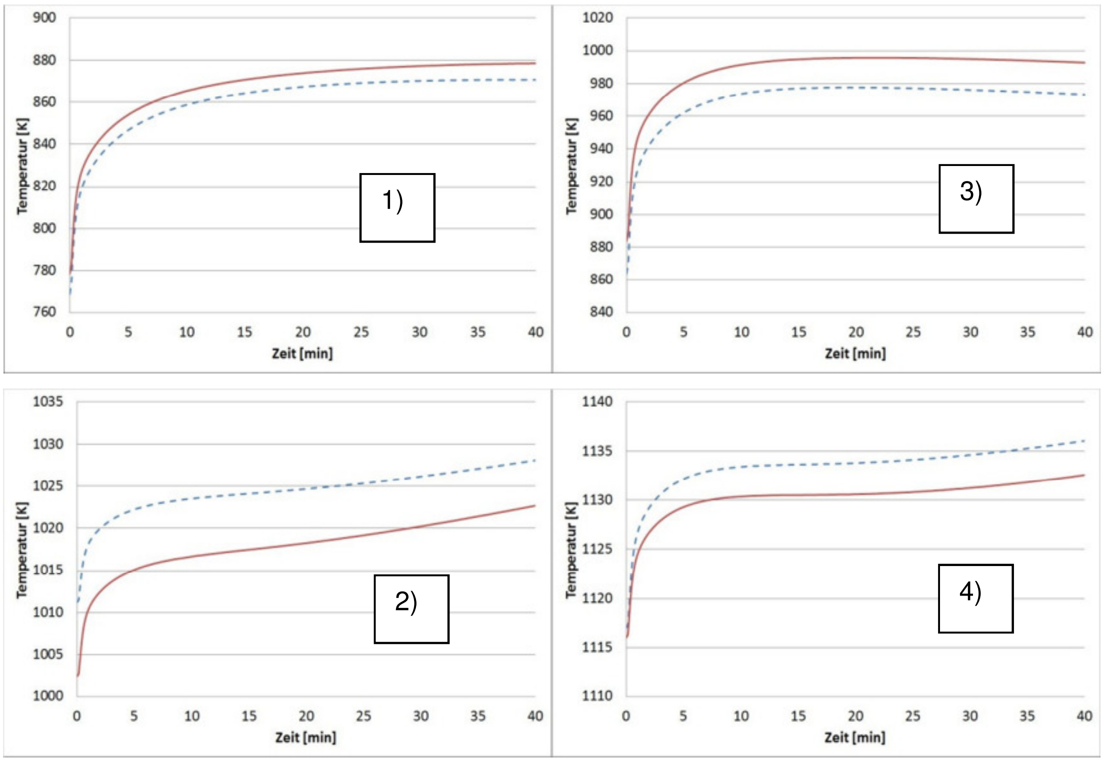

Figure 32: Maximum fuel temperature, compare to densified (red) and non densified pebble bed (blue): 1) case 1, 2) case 2, 3) case 3, 4) case 4.

For case 1 and 3, the temperature evolutions are dominated by the generated power in the zones, after a short temperature maximum in case 2 and 4 (in case 4 more pronounced), the hot spots are further heated by the hot gas coming from the pebble bed above the densification.

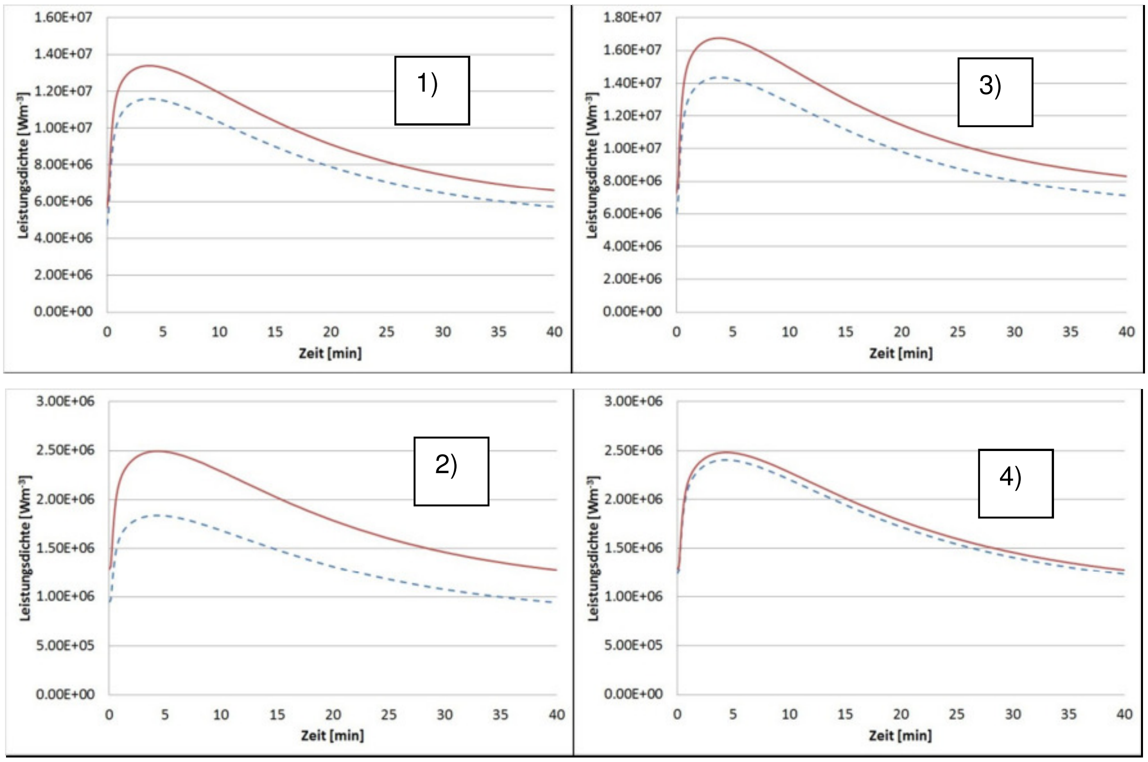

Figure 33: Power density of densified (red) and non densified pebble bed (blue): 1) case 1, 2) case 2, 3) case 3, 4) case 4.

The maximum fuel temperature in the densification cluster over time is plotted in Figure 32. In the densified regions in the middle of the core, the temperatures are slightly increased compared to the undisturbed pebble bed; in the densified regions at the bottom, it is the opposite case. This effect is produced through the moving of the hotspot with the maximum fuel temperature towards the location of the power maximum. The phenomenon is caused by the influence of the undensified pebble bed on the power density, which profiles are shifted towards the top.

Figure 33 shows the comparison of the power density over the time in the densification clusters and the maximum temperature. The influence on the power density is dominated by the feedback of the fuel temperature on the power. The effect in case 2 is the biggest, however the absolute value of the power density in case 3 is the biggest due to the maximum power and flux.

3.2.4 Asymmetric control rod withdrawal with densifications

To continue the investigation an asymmetric control rod withdrawal of 3 control rods at the same position as in a control rod ejection was executed. For that the velocity was reduced to 1 cm/s. The results with the ejection in general display the same tendency; but through the smaller inserted reactivity the maximum power and temperature are lower. The temperature increase is around 20 K. The maximum power occurs at 39 s.

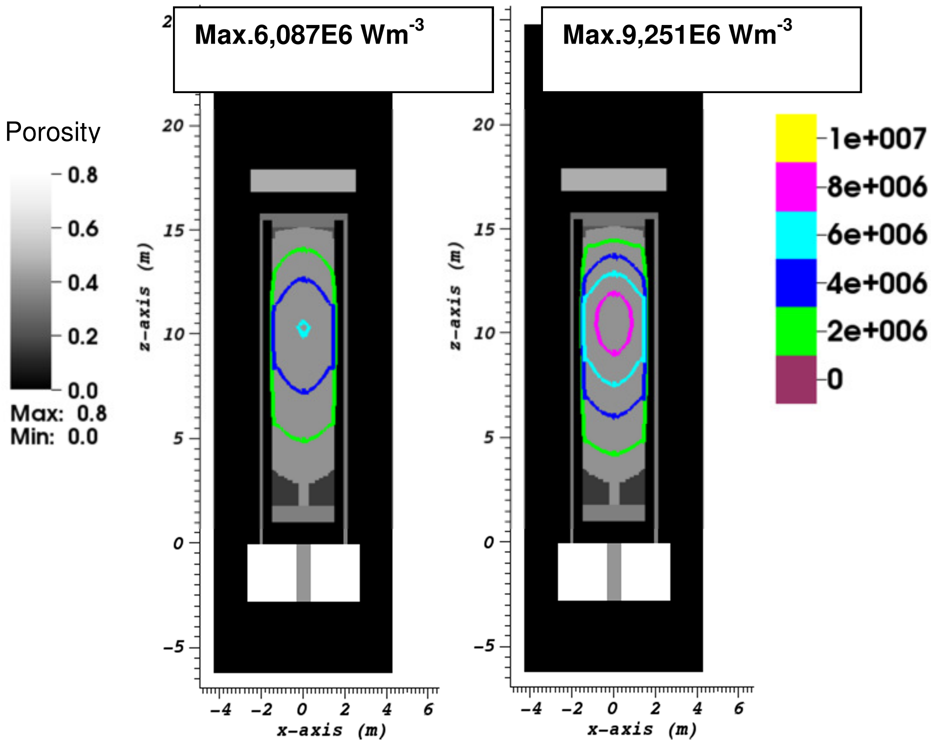

Figure 34: Power distribution at the beginning (0 s, left) and at the maximum power time (39 s ,right) for a one side control rod withdraw, without densification.

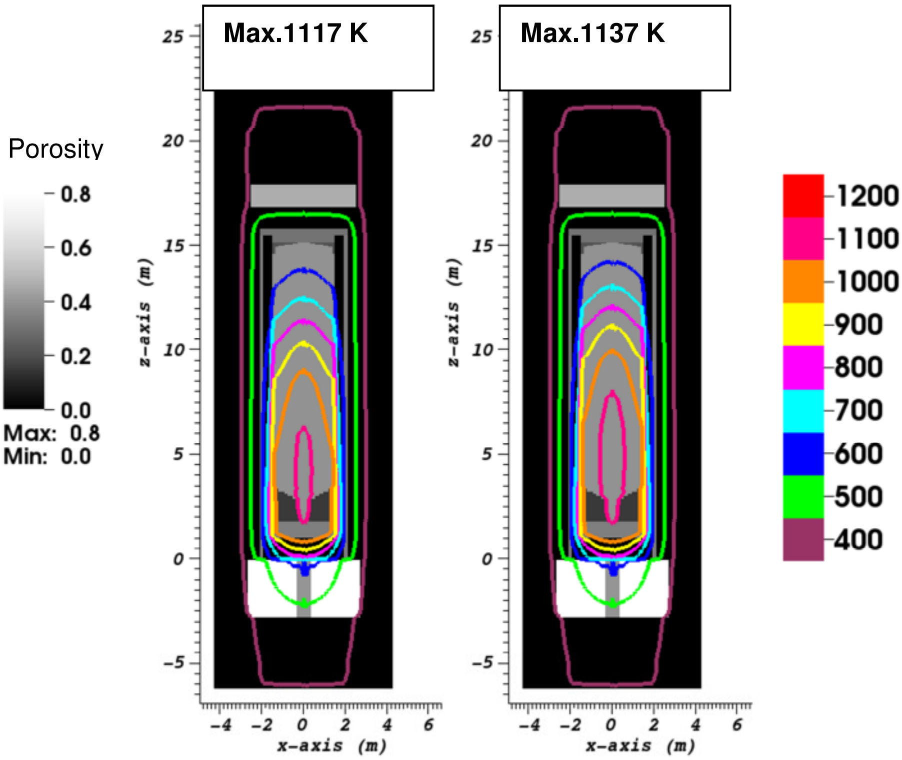

Figure 35: Maximum fuel temperature distribution at the beginning (0 s, left) and at the end (45 s, right) of the transient for a one side control rod withdraw, without densification.

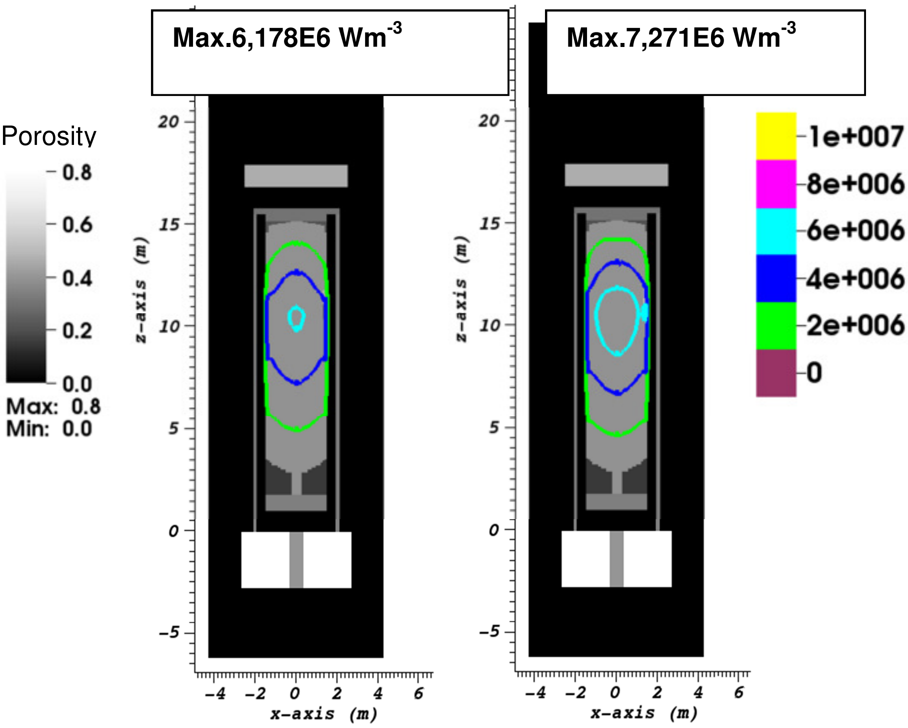

Figure 36: Power distribution at the beginning (0 s, left) and at the maximum power time (39 s, right) for a one side control rod withdraw, densification at the maximum power height, edge region.

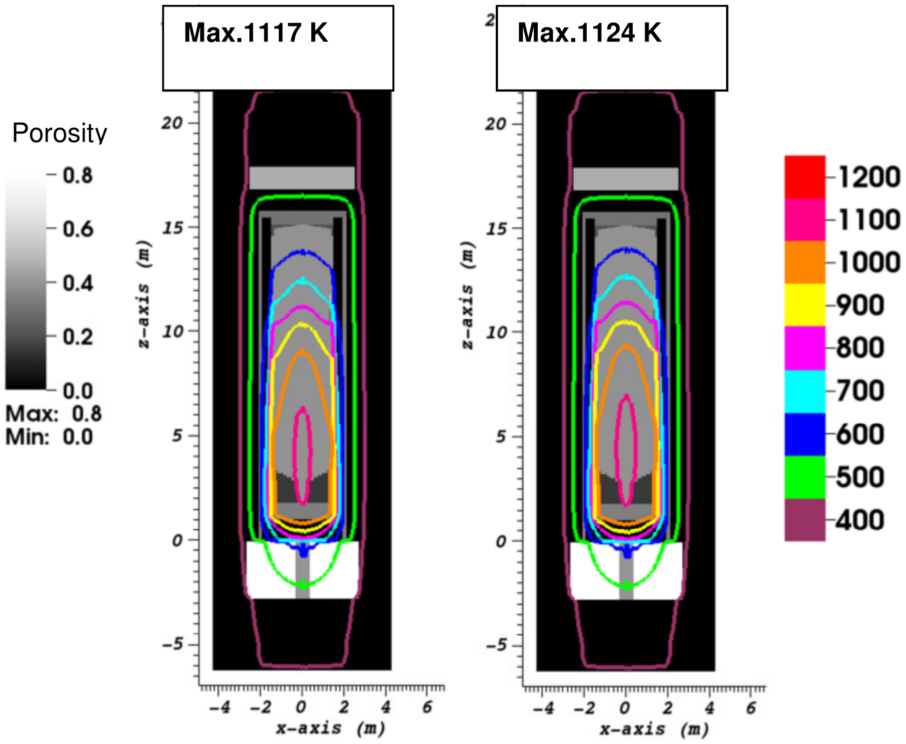

Figure 37: : Maximum fuel temperature deistribution at the beginning (0 s, left) and at the end (45 s, right) of the transient for a one side control rod withdraw, densification at the maximum power height, edge region.

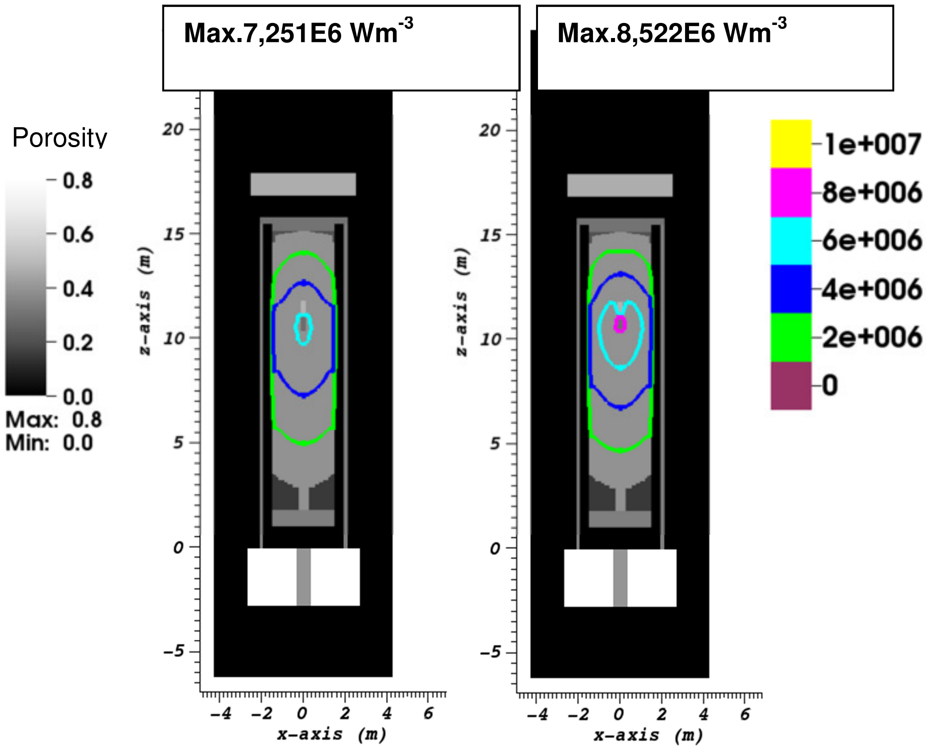

Figure 38: power distribution at the beginning (0 s, left) and the maximum power time (40 s, right) for a one side control rod withdraw, densification at the maximum power height, middle

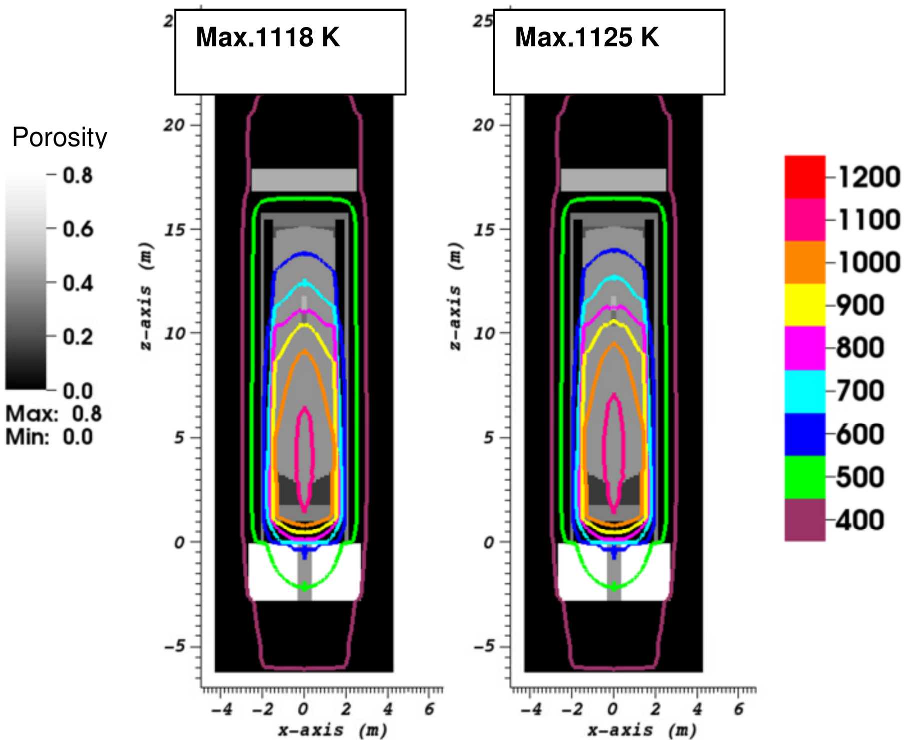

Figure 39: maximum fuel temperatureat the beginning (0 s, left) and end (40 s, right) of the transient for a one side control rod withdraw, densification at the maximum power height, middle.

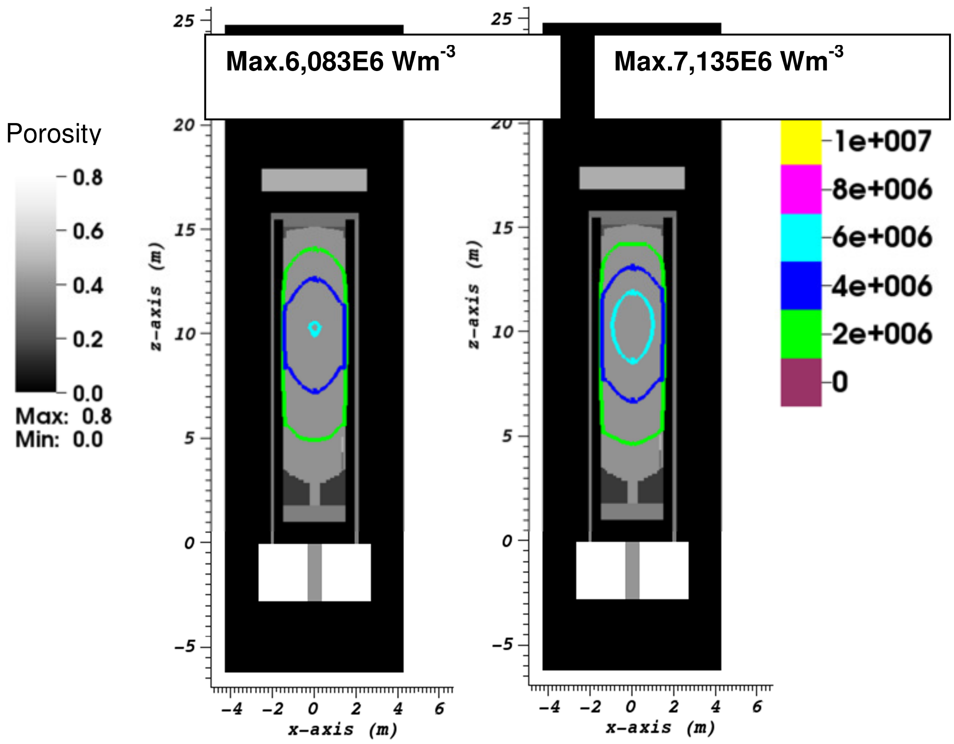

Figure 40: Power distribution at the beginning (0 s, left) and at the maximum power time (39.5 s, right) for a one side control rod withdraw, densification close to the bottom, edge region.

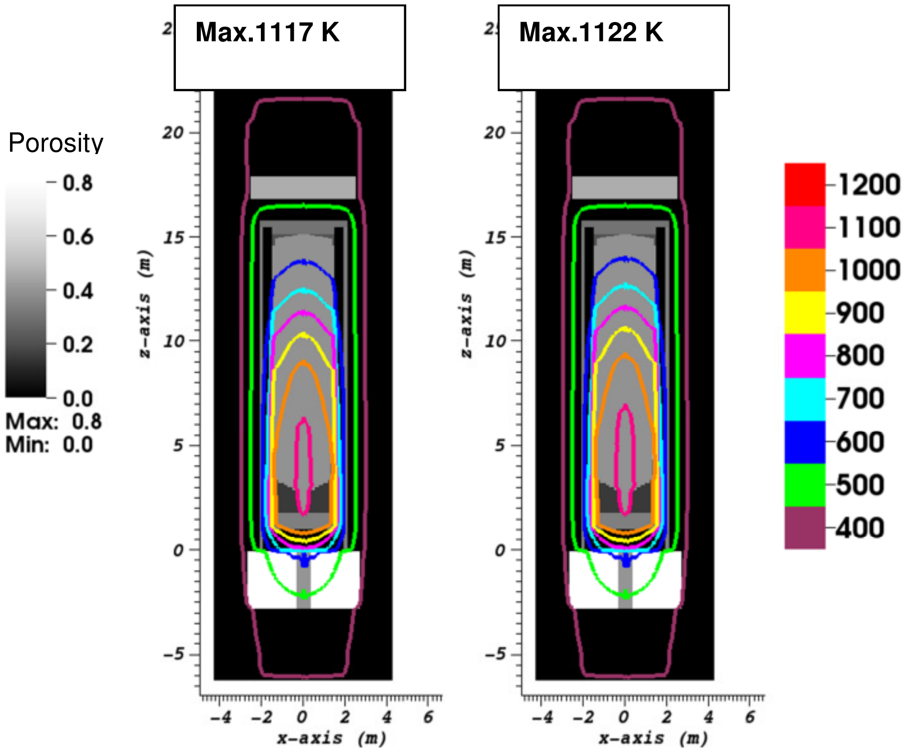

Figure 41: Maximum fuel temperature distribution at the beginning (0 s, left) and at the end (45 s, right) of the transient for a one side control rod withdraw, densification close to the bottom, edge region.

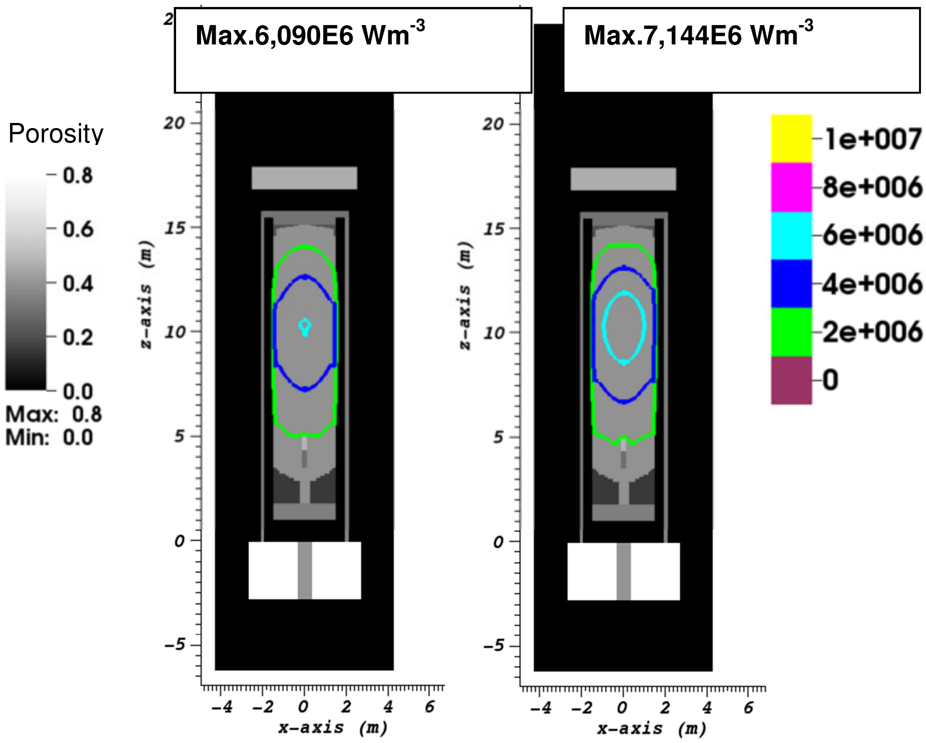

Figure 42: Power distribution at the beginning (0 s, left) and at the maximum power time (39.5 s, right) for a one side control rod withdraw, densification close to the bottom, middle.

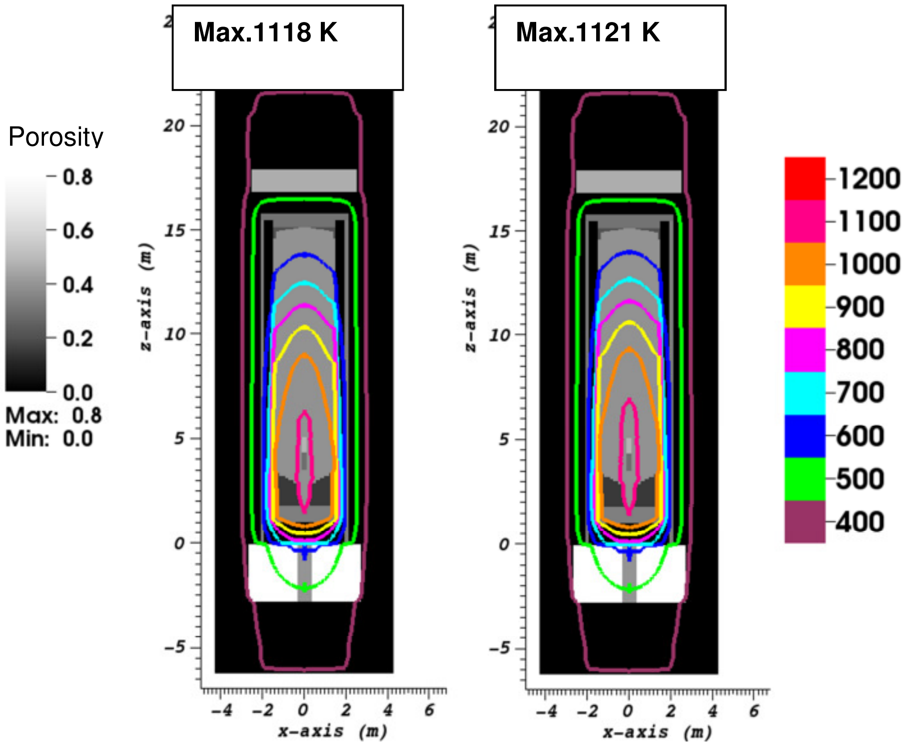

Figure 43: Maximum fuel temperature distribution at the beginning (0 s, left) and at the end (45 s, right) of the transient for a one side control rod withdraw, densification close to the bottom, middle.

3.3 The total control rod ejection scenario

The worst case of the ejection and withdrawal cases is the ejection (0.1 s) of all of the control rods at the same time. Since the rods are inserted 4.6 metres from the top reflector the ejection speed is 46 m/s. The hottest part for this case lies on the centreline of the core. This fast ejection scenario assumes a total destruction of the control rod drives where the rods are ejected from the system with 60 bars against ambient pressure.

Since the ejection time of 0.1 seconds is very small, the maximum time step size for the transient in the first second is 0.0025 seconds, before it is increased to 0.05 seconds after the first 3 seconds. Selecting a time step size this small, the ejection time is subdivided in 40 steps. This time step size should be small enough to cover the short-term processes taking place.

Previous analysis indicated that no inadmissible temperature rise to the fuel occurs. When analysing the fuel kernel temperatures assuming one average fuel type, the maximum temperature criterion of 1620℃ is not exceeded. However, if the introduced modifications of distinction of the fuel pass number is used, the hottest fuel kernel will exceed this temperature (~2100℃), but only for a very short time (less than 10 seconds).

The power increases by a factor of ~10 in less than a second, as shown in Figure 44 and Figure 45. The maximum power value of 24,166 MW is reached after 0.79 seconds after start of the transient or 0.69 seconds after control rods were ejected. The corresponding maximum kernel temperatures, average fuel and moderator temperatures are shown in Figure 46.

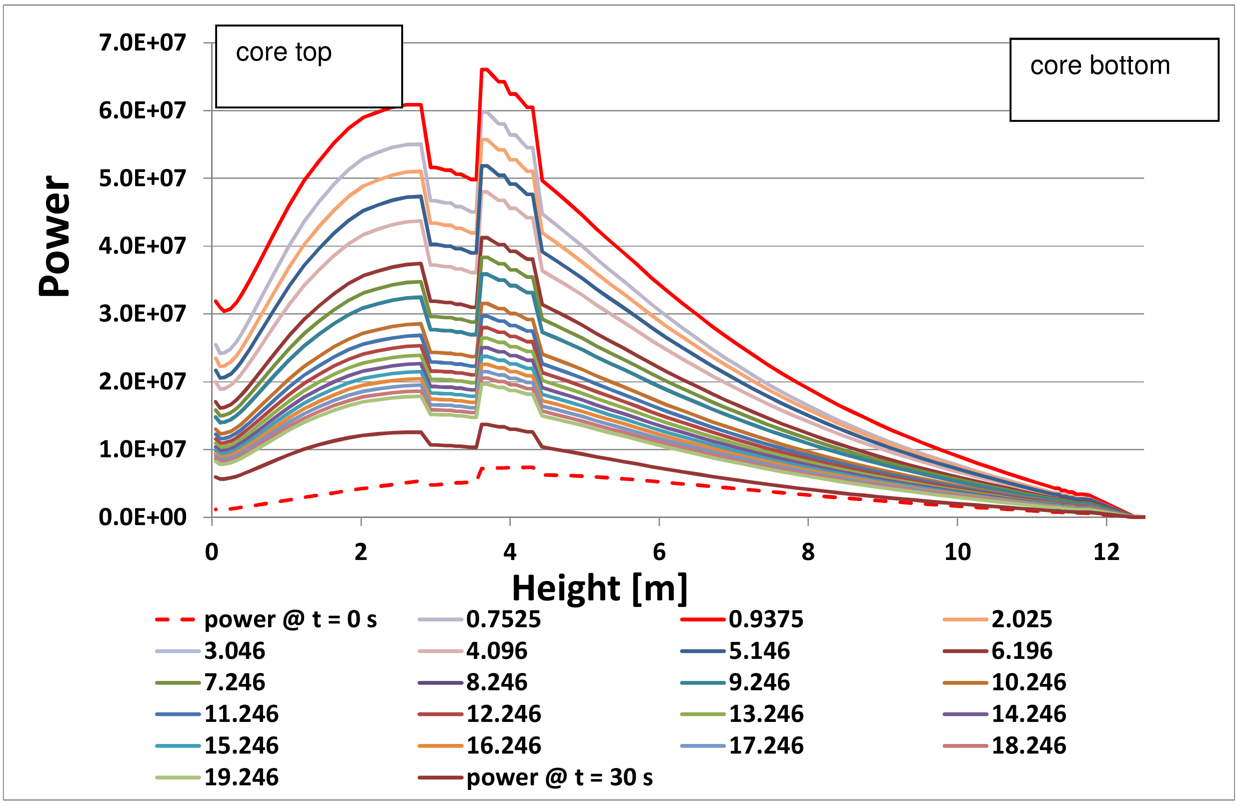

Figure 44 : Power density at the centreline for a total control rod ejection for different times

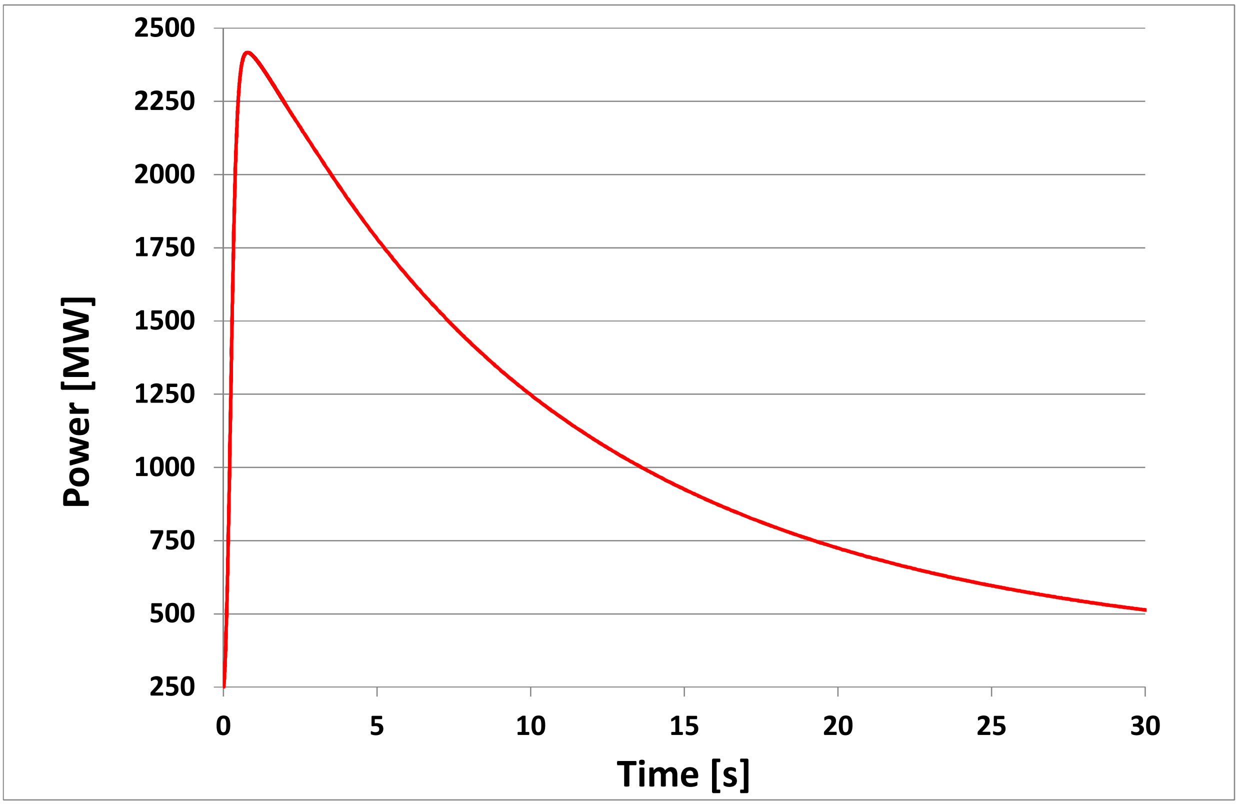

Figure 45 : Total power evolution for a total control rod ejection scenario of the HTR-PM, the maximum power is reached after 0.79 seconds after the beginning of the ejection

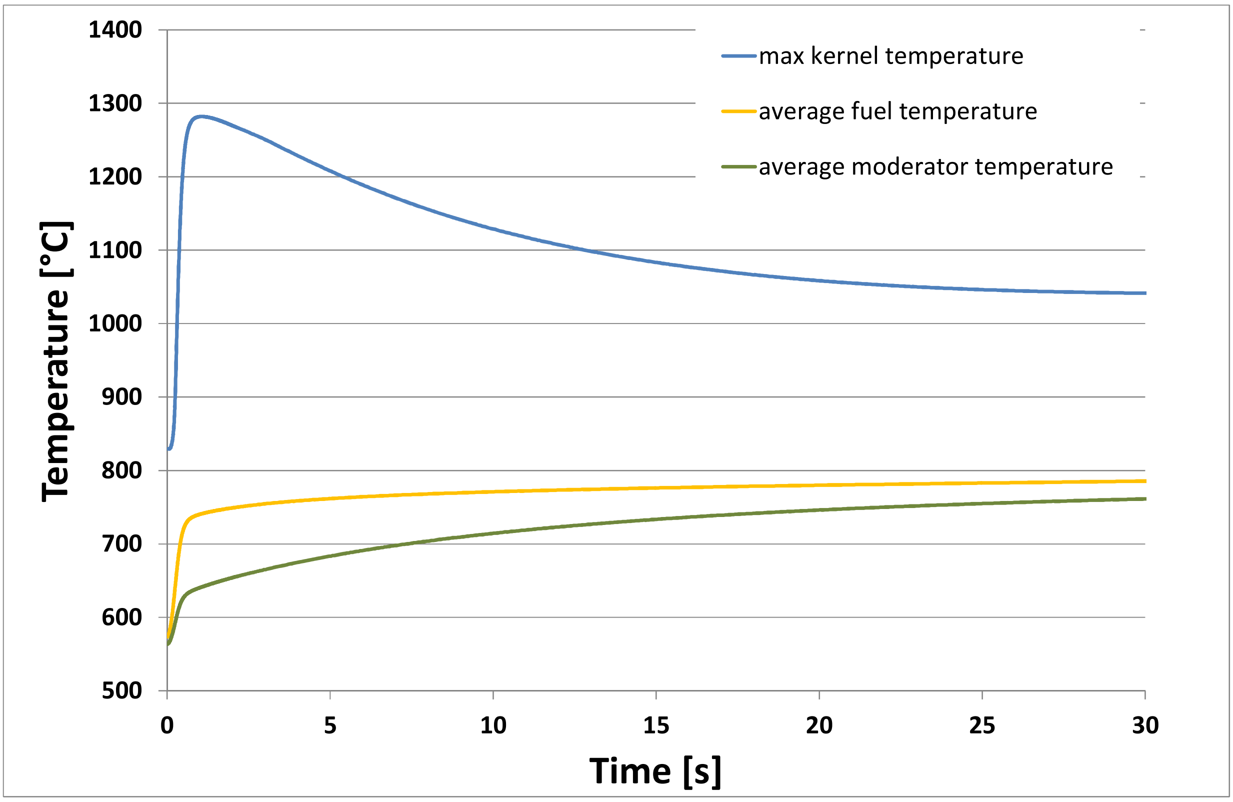

Figure 46 : Temperature evolution for a total control rod ejection case for the maximum kernel temperature, average fuel and average moderator temperatures.

3.4 Modifications in ATTICA^{3D} to account for cycle number

The HTR-PM loading pattern for fuel elements foresees fifteen core passes before the pebbles are discharged. Assuming a random uniform distribution, the pebbles in the pebble bed are arranged homogeneously such that if a random batch of pebbles would be extracted a mean number of each core pass can be expected. This was also assumed when the temperatures of the fuel elements were calculated.

Now, modifications are introduced into ATTICA^{3D} to be able to account for different heating powers of a fuel element according to its core pass number.

The reason for this modification is the fact that fresh pebbles do contain most of the fuel and has the least burn-up, i.e. fission product content and, hence, the lowest decay heat production. So in nominal operation the highest temperatures can be expected for a fresh fuel element. When decay heat comes into play, the highest temperatures will occur in the fuel pebbles that experienced the highest burn-up.

The new model in ATTICA^{3D} allows the user to provide different heating powers per fuel pass. Starting from the assumption that each computational mesh contains a fraction of fuel elements, the total volume of pebbles within the pebble bed amounting is proportional to each cycle, that is 1/15. This heating power was varied assuming the power factors presented in Table 5. These power factors have been evaluated from steady-state analysis with the ZIRKUS system and represent values averaged over the whole core. The power factors for the pebbles are given relative to the mean power production where no distinction per fuel cycle was done. Hence, these power factors were all 1.

Table 5 : Power factors for fuel pebbles

Fuel pass	Power factors
1	1.9
2	1.7
3	1.5
4	1.3
5	1.1
6	1.05
7	1.02
8	1
9	0.98
10	0.95
11	0.9
12	0.7
13	0.5
14	0.25
15	0.15

These new power factors are global values meaning they are applied to every computational mesh of ATTICA^{3D}, thus far, omitting possible local variations of the factors. The temperature of each distinct pebble core pass are taken and averaged together according to their mean volume in the pebble bed. This approach yields 15 different fuel temperatures. The values were estimated from previous experience where power factors have been determined for a 15 core pass fuel cycle. The maximum power value of 1.9 is not expected to be too high, but will still be verified for the HTR-PM. Also, from previous works done in the framework of the PUMA project, the predecessor of the ARCHER it was found that the mean spectrum is approximated best by an ensemble of pebbles (mixture) and that single pebble spectrum calculations that are later weighted and mixed are much less suitable to describe the spectrum, realistically. Therefore, a modification of the interface for TORT-TD and ATTICA3D to instantaneously feed-back the fuel temperatures to the neutronics for each core pass number was considered not necessary. Therefore the power factors will also be kept constant for the duration of the transient

For demonstration purposes of the new fuel temperature model, a steady-state TORT-TD/ATTICA^{3D} analysis is performed without a densification (Figure 47), with a densified region in the ATTICA^{3D} domain, omitting the densification for the TORT-TD neutronics model and with a densified region in both the TORT-TD and ATTICA^{3D} simulation model.

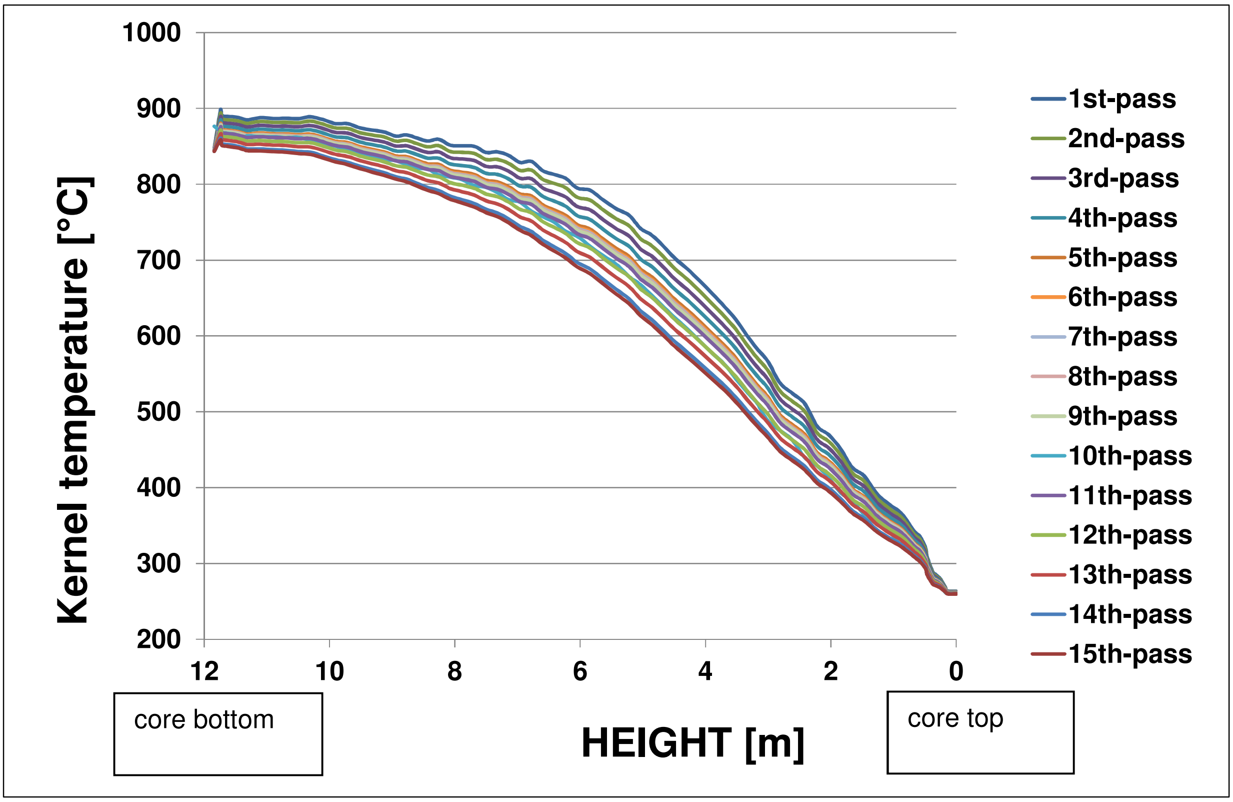

Figure 47 : Steady state fuel temperatures per core pass without densified region

The maximum temperature difference between the first and the last core pass of a pebble with the power factors from above is 118 K at about 4.5 metres from the top of the core. Including a densification in the thermal fluid dynamic part only, a more densified region (28.75 %) is located in the power maximum while a less densified region (47.6 %) is located above or below the densified cluster to preserve the pebble mass within the core cavity without increasing or decreasing the core height.

For the result with a densified cluster of ATTICA^{3D}, the maximum temperature difference of between the first and the last core pass amounts to 136 K, see Figure 48.

The results of densified clusters in both, neutronics and thermal fluid dynamics, are shown in Figure 49. The maximum fuel temperature difference between the first and the last core pass reduces to 130 K again. The centreline temperatures of the different core pass numbers are shown together with the centreline power.

All results with a densification modelled in both neutronics and thermal fluid dynamics or in thermal fluid dynamics only do not display any significantly higher temperatures for steady state. Therefore it is concluded that a densification in the power maximum will not lead to inadmissibly high fuel temperatures if the pebbles can be assumed to be mixed homogeneously.

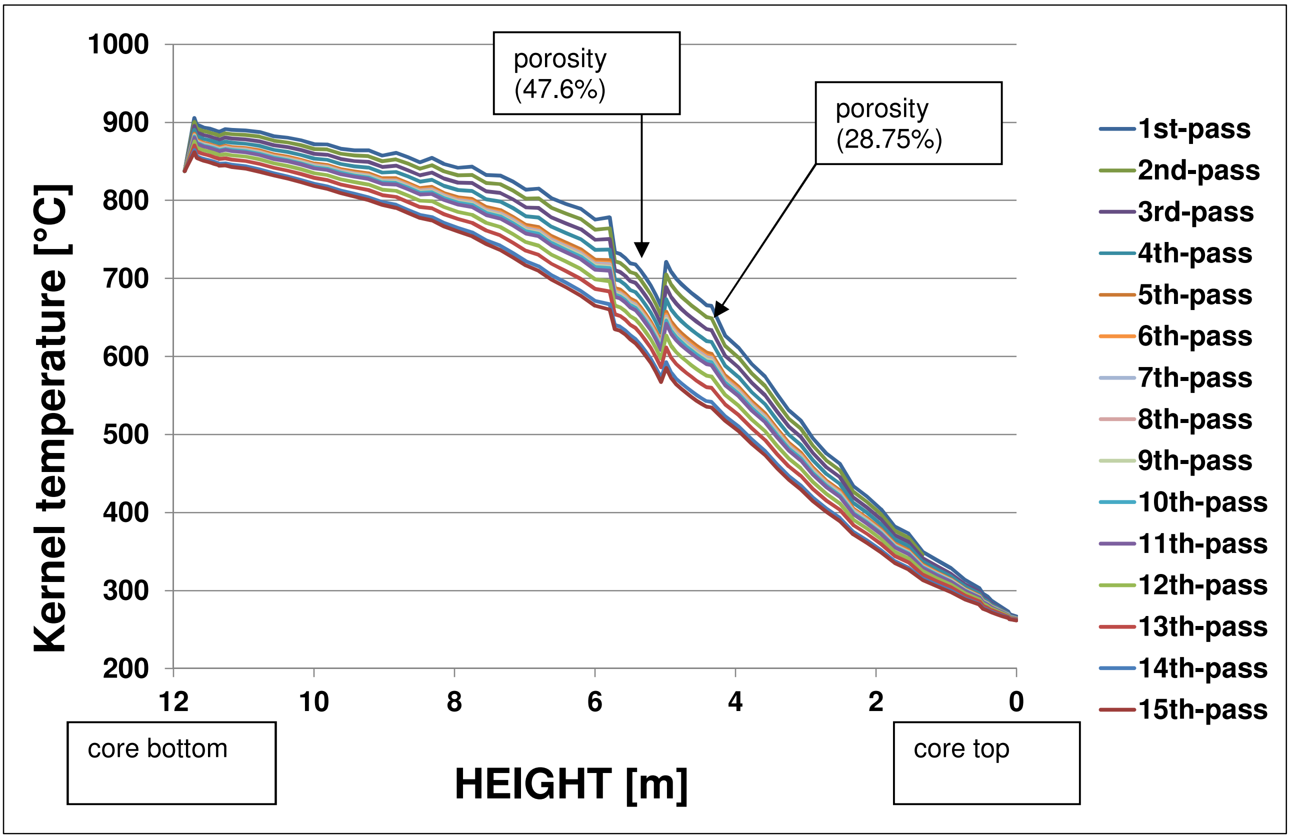

Figure 48 : Coupled TORT-TD/ATTICA^{3D} results with a densification in the thermal fluid dynamics only

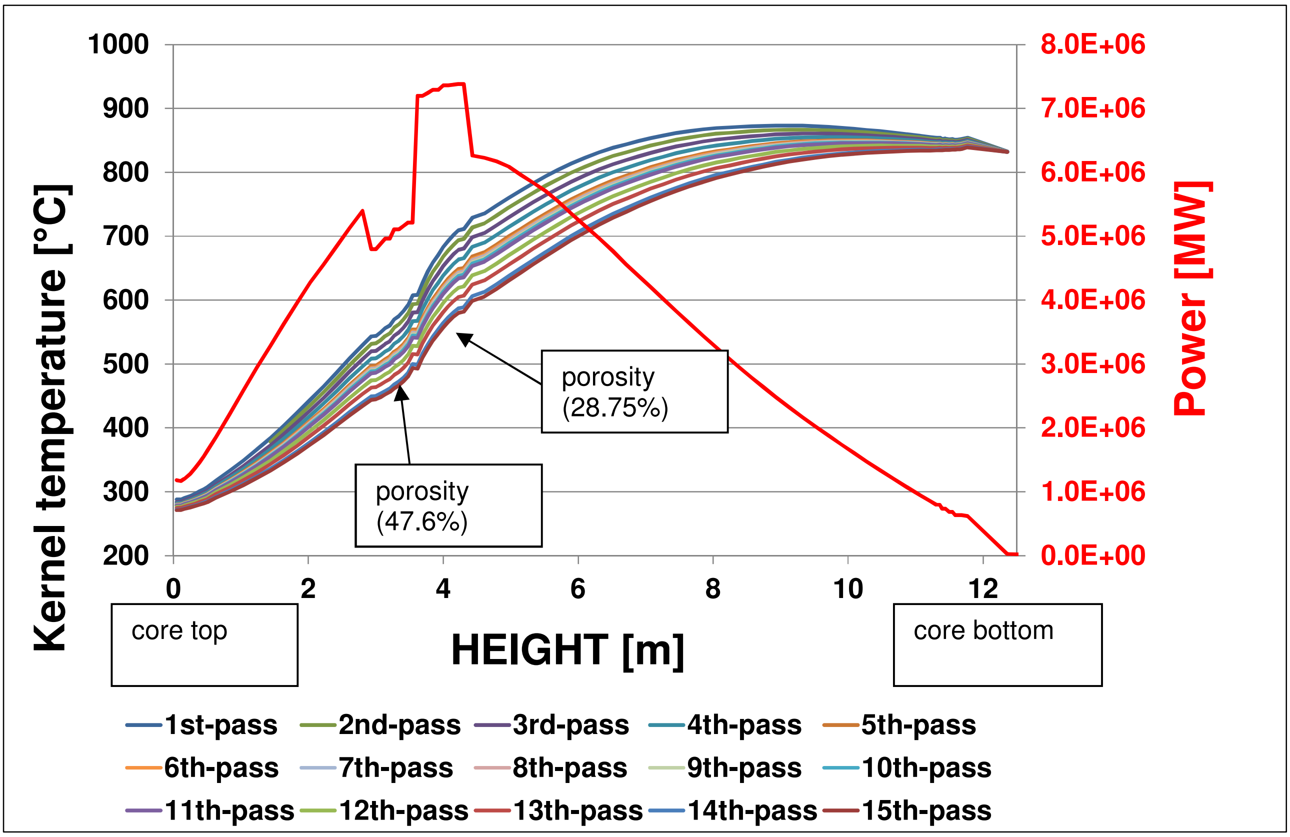

Figure 49 : Coupled TORT-TD/ATTICA^{3D} steady state calculation with a more and less densified cluster of pebbles, left axis : fuel kernel temperatures on the centreline, right axis : power density on the centreline (red)

3.5 Impact of the new fuel-pass model on the results of the total control rod ejection scenario

For the considered worst case scenario of the total control rod ejection case, the power increase remains the same since the mean fuel and moderator temperatures do not differ. However, for the strong reactivity increase (1.3%) caused by the ejected control rods, the maximum fuel temperature results differ significantly. The integral power evolution is the same as shown in Figure 45 reaching a power increase factor around 10, but the maximum fuel kernel temperature increase drastically, see Figure 50. Instead of 1,281 ℃ in the previous analysis, the case with the fuel pass model reaches **2,241 ℃** after 0.9375 seconds. This is much higher than the temperature for the previous case. After less than 10 seconds, the maximum fuel kernel temperature is already below 1600℃, again.

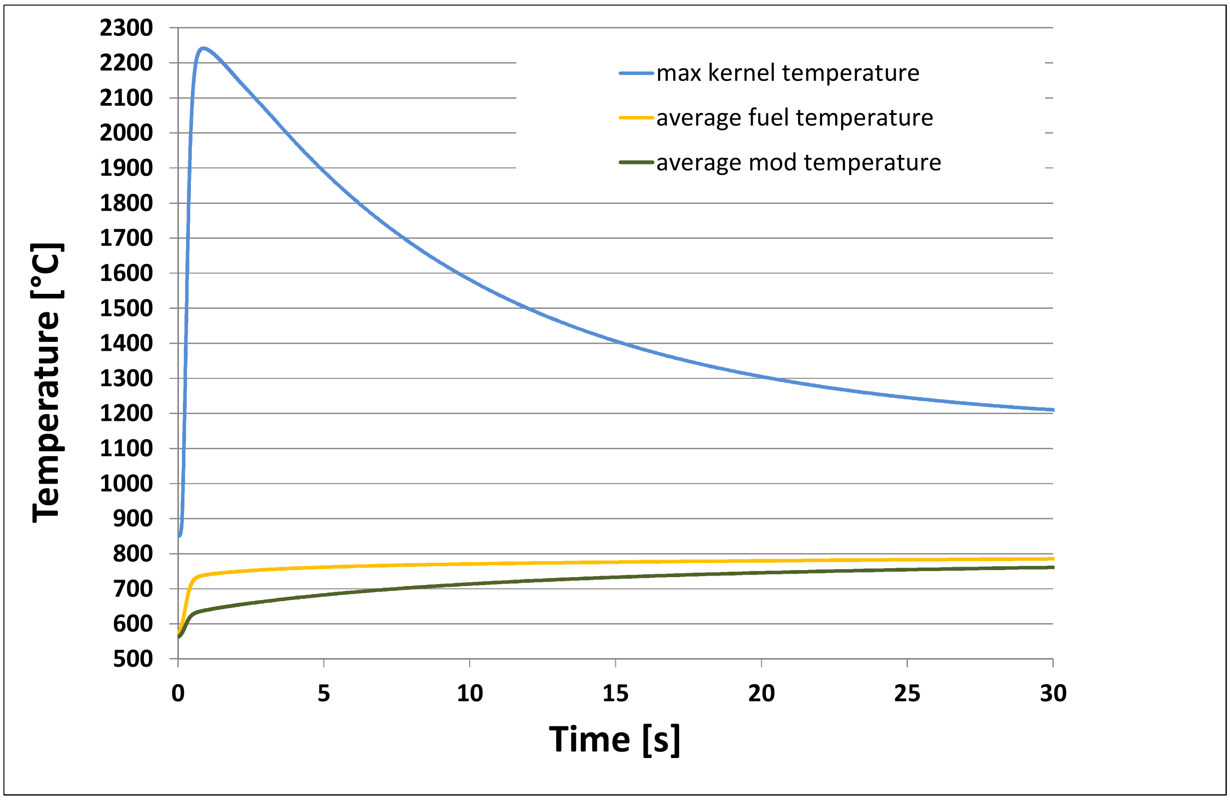

Figure 50 : Maximum kernel temperature and average fuel and moderator temperatures for the total control rod ejection case.

The fuel temperature model is now analysed at 0.9375 seconds, the time where the maximum temperature is reached, see Figure 51. There, the difference in the maximum fuel kernel temperatures reaches over 1,500 K between the first and the last core-pass with the assumed power factors. For the axial location with the highest temperatures obtained, the temperature distribution over the spherical fuel element is presented for both the graphite and the UO_2-kernels, see Figure 52. Starting from the outermost shell at approximately 500℃ the centre of the innermost kernel reaches 2,241℃ leading to a temperature difference between the surface and the hottest particle of 1,700 K!

These values for the fresh fuel elements are inadmissibly high and this extreme transient case must be prevented due to appropriate design measures, i.e. limitation of ejection speed or restriction of the maximum rod number to be ejected (like in a LWR where the most effective rod can be ejected). Since the fresh fuel element has no significant amount of fission gases, the inner fission gas pressure might be low enough to stand this transient. This, however, must be evaluated by experiment and fuel performance specialists.

A remedy can be the reduction of core-passes that will reduce the spread of the power factors. But this will also lead to a reduction of maximum burn-up.

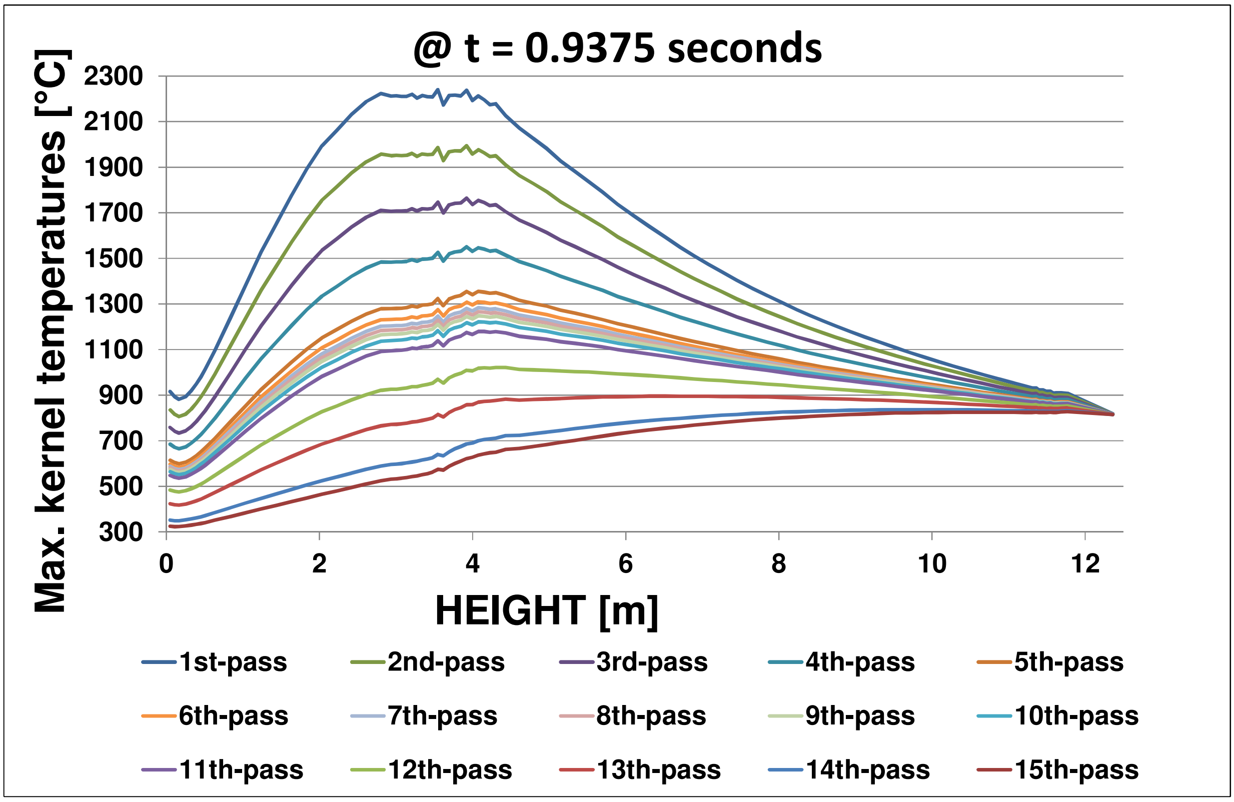

Figure 51 : Distribution of maximum fuel kernel temperatures at the centreline for a total control rod ejection at t = 0.9375 seconds, time of maximum temperature.

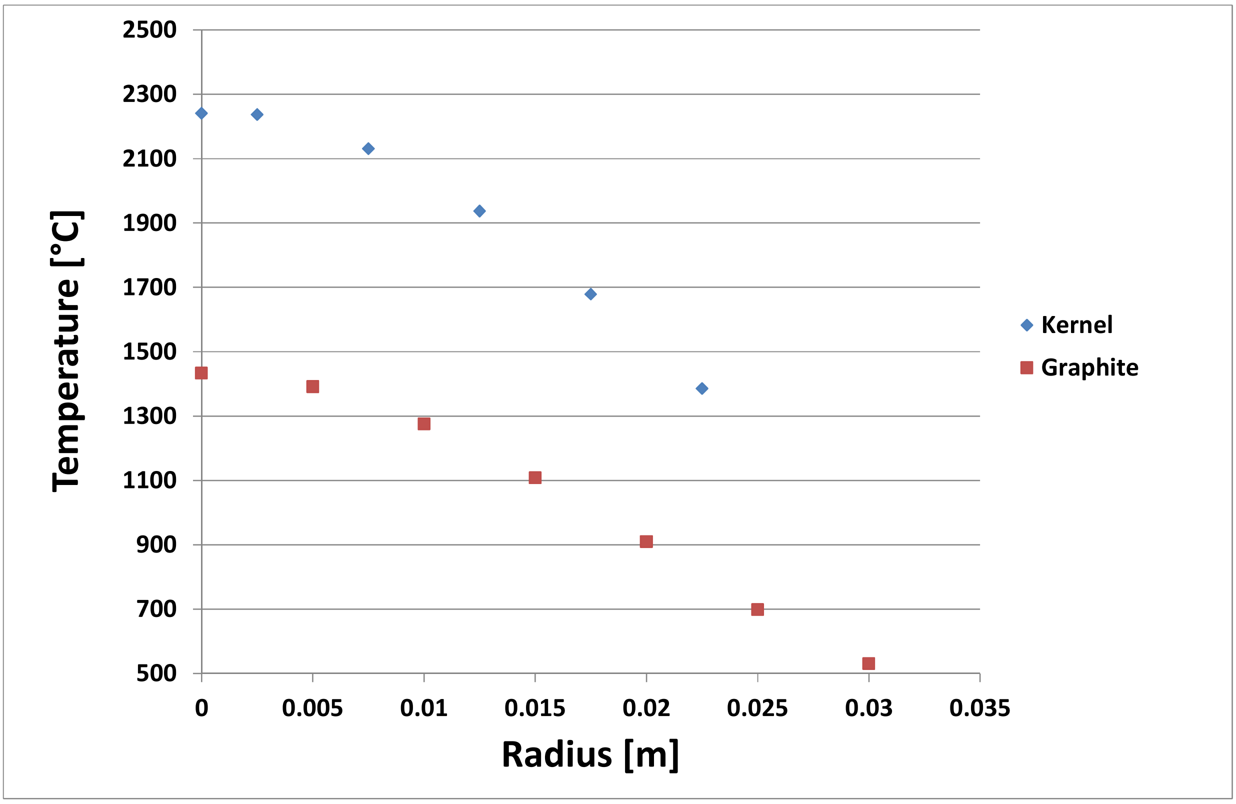

Figure 52 : Temperature distribution of the kernel and shell temperature over the hottest fuel element

4 Summary and outlook

In the first chapters 2 and 3 the tools to be used as well as the reference plant (HTR-PM) were specified. In chapter 4 the methodology to simulate densifications within a pebble bed is addressed including the approach used to modify macroscopic cross sections for the densified pebble clusters.

Then, the hotspot analysis was performed for the depressurised loss of forced cooling accident as well as several control rod ejection and withdrawal cases with 3 out of 8 control rods ejected. It could be shown that for the cases simulated the densification do not lead to inadmissibly high temperatures. Moreover, if the pebble bed is considered to be a mixture of pebbles without resolution of the respective core-pass number, the results may cover the hottest part by means of averaging.

This analysis has been performed for an ensemble of pebbles, i.e. for a cluster of pebbles with different number of core passes. The HTR-PM concept foresees 15 fuel pebbles core passes, thereby reaching the design burn-up of 90 MWd/kg of HM. Since fuel spheres, at the beginning, have a much higher content of fissile material, the produced power, and hence, the fuel temperatures will also be much higher.

This investigation was performed in the updated version of this deliverable, for the total control rod ejection the maximum fuel kernel temperature was determined to be 2,241℃. This temperature is already way beyond the licensing temperature. It is questionable if such a scenario has to be realistically dealt with for licensing purposes. A transient with reduced ejection speed (100 cm/s), as in the HTR-Module reactor will also be analysed in the next submittal.

For more detailed analysis, the ZIRKUS system will be used to determine local power factors of fuel elements of different core pass numbers.

A case of fresh pebbles clustering at spots with high powers is also planned. For this analysis, the reload module for pebbles will have to be manipulated and new macroscopic cross sections have to be generated.

5 Annexes

Annex 1 – Document approval by beneficiaries' internal QA

5.1 Annex 1: Document approval by beneficiaries' internal QA

Fill involved beneficiaries as appropriate (mandatory for Milestones and Deliverables, but optional for other document type)

#	Name of beneficiary	Approved by	Function	Date
1				
2				
3				
4				
6				
7				
8				
9				
10				
11				
12				
13				
14				
15				
16				
17				
18				
19				
20				
21				
22				

5.2 References

[1] W. Bernnat, W. Feltes, **Models for reactor physics calculations for HTR pebble bed modular reactors**, Nuclear Engineering and Design 222 (2003) 331–347

[2] D. Mathews, **An Improved Version of the Microx-2 Code**, Paul Scherer Institut, PSI Bericht Nr. 97-11, November 1997.

[3] X-5 Monte Carlo Team, **MCNP – A General Monte Carlo N-Particle Transport Code, Version 5, Los Alamos National Laboratory**, LA-UR-03-1987, revised 10/3/05.

[4] Rhoades, W. A., Simpson, D. B. (1991). **The TORT Three dimensional Discrete Ordinates Neutron/Photon Transport Code (TORT Version 3)**, ORNL/TM-13221.

[5] A. Seubert, K. Velkov and S. Langenbuch, **The Time-Dependent 3-D Discrete Ordinates Code TORT-TD with Thermal-Hydraulic Feedback by ATHLET Models**, Physor 2008, Interlaken, Switzerland, September 14-19, 2008.

[6] Seubert, A. Sureda, J. Bader, J. Lapins, M. Buck, E. Laurien, **The 3-D time-dependent transportcode TORT-TD and its coupling with the 3D thermal-hydraulic code ATTICA^{3D} for HTGR applications**, Nucl. Eng. and Design 2011, in press.

[7] The Nuclear Safety Standards Commission (Kerntechnischer Ausschuss - KTA), **Reactor Core Design for High-Temperature Gas-Cooled Reactor**, KTA 3102, 1983.

[8] H. Reutler and G.H. Lohnert, **ADVANTAGES OF GOING MODULAR IN HTRs**, Nuclear Engineering and Design 78 (1984) 129-136.

[9] Zuoyi Zhang, Zongxin Wu, Dazhong Wang, Yuanhui Xu, Yuliang Sun, Fu Li , Yujie Dong, **Current status and technical description of Chinese 2×250MWth HTR-PMdemonstration plant**, Nuclear Engineering and Design 239 (2009) 1212–1219.

[10] Yanhua Zheng, Lei Shi, Yujie Dong, **Thermohydraulic transient studies of the Chinese 200 MWe HTR-PM for loss of forced cooling accidents,** Annals of Nuclear Energy 36, pp 742–751, 2009.

[11] Rainer Moormann, **A safety re-evaluation of the AVR pebble bed reactor operation and its consequences for future HTR concepts*,*** Forschungszentrum Jülich Jül-4275, Juni 2008.

[12] Association of German Engineers (VDI) - Society for Energy Technologies (Publ.), **AVR-Experimental High-Temperature reactor; 21 years of successful operation for a future energy technology**, page 154ff, VDI-Verlag GmbH, Düsseldorf 1990.

[13] G.J. Auwerda, J.L. Kloosterman, D. Lathouwers, T.H.J.J. van der Hagen: **Macroscopic and Microscopic Packing Properties of Experimental and Computational Pebble Beds**, Nuclear Technology (2013). Submitted

[14] DIN 25485**: Berechnung der Nachzerfallsleistung der Kernbrennstoffe von Hochtemperaturreaktoren mit kugelförmigen Brennelementen (English: German Industrial**

Standard, Calculation of decay heat for fissile material of high temperature reactors with spherical fuel elements), Mai 1990.

[15] F. Reitsma, K. Ivanov, T. Downar, H. de Haas, H. D. Gougar: **The OECD/NEA/NSC PBMR Coupled Neutronics/Thermal Hydraulics Transient Benchmark: The PBMR-400 Core Design**, Proceedings of PHYSOR 2006, Canadian Nuclear Society, (14.-16. September 2006)